

INFORMATION TO USERS

This manuscript has been reproduced from the microfilm master. UMI films the text directly from the original or copy submitted. Thus, some thesis and dissertation copies are in typewriter face, while others may be from any type of computer printer.

The quality of this reproduction is dependent upon the quality of the copy submitted. Broken or indistinct print, colored or poor quality illustrations and photographs, print bleedthrough, substandard margins, and improper alignment can adversely affect reproduction.

In the unlikely event that the author did not send UMI a complete manuscript and there are missing pages, these will be noted. Also, if unauthorized copyright material had to be removed, a note will indicate the deletion.

Oversize materials (e.g., maps, drawings, charts) are reproduced by sectioning the original, beginning at the upper left-hand corner and continuing from left to right in equal sections with small overlaps.

Photographs included in the original manuscript have been reproduced xerographically in this copy. Higher quality 6" x 9" black and white photographic prints are available for any photographs or illustrations appearing in this copy for an additional charge. Contact UMI directly to order.

Bell & Howell Information and Learning
300 North Zeeb Road, Ann Arbor, MI 48106-1346 USA
800-521-0600

UMI[®]

RECHARGE ESTIMATES OBTAINED FROM CENTRIFUGE MEASUREMENTS.

ABO ARROYO, NEW MEXICO

A Thesis

Presented to

The Faculty of the Department of Geology

San Jose State University

In Partial Fulfillment

of the Requirements for the Degree

Master of Science

by

Angus M. Lewis

December 2000

UMI Number: 1402522

UMI[®]

UMI Microform 1402522

Copyright 2001 by Bell & Howell Information and Learning Company.

All rights reserved. This microform edition is protected against
unauthorized copying under Title 17, United States Code.

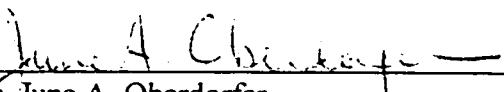
Bell & Howell Information and Learning Company
300 North Zeeb Road
P.O. Box 1346
Ann Arbor, MI 48106-1346

© 2000

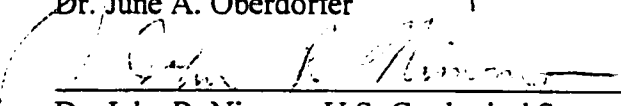
Angus M. Lewis

ALL RIGHTS RESERVED

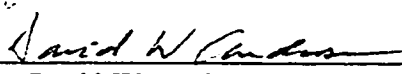
APPROVED FOR THE DEPARTMENT OF GEOLOGY



Dr. June A. Oberdorfer

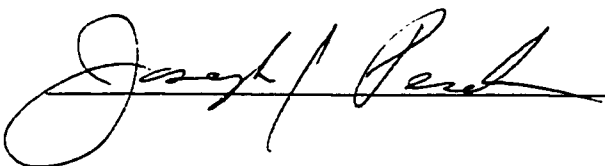


Dr. John R. Nimmo, U.S. Geological Survey



Dr. David W. Andersen

APPROVED FOR THE UNIVERSITY



ABSTRACT

RECHARGE ESTIMATES OBTAINED FROM CENTRIFUGE MEASUREMENTS, ABO ARROYO, NEW MEXICO

by Angus M. Lewis

Through measurement of unsaturated hydraulic conductivity (K) using the steady-state centrifuge method, point recharge estimates have been obtained at 11 locations in and adjacent to a 28-km reach of Abo Arroyo. Core samples were collected from depths where soil-moisture fluctuations are assumed negligible, so that downward water flow is steady and driven by gravity alone. At this depth, the value of K at the field water content of the core sample can be interpreted as a point recharge rate. Recharge appears to be significant at locations within Abo Arroyo (channel recharge), ranging from 0.12 to 2700 cm/yr, whereas recharge at locations 3.5 to 500 m away from the arroyo (inter-arroyo recharge) is less than 0.015 cm/yr. Integration of point recharge estimates through interpolation and geologic interpretation results in a total recharge estimate of 1300 acre-ft/yr within Abo Arroyo and 970 acre-ft/yr over the entire inter-arroyo region of the basin.

ACKNOWLEDGEMENTS

I thank Dr. John Nimmo of the U.S. Geological Survey for providing me with an opportunity to work on this project, and I thank both Dr. June Oberdorfer and Dr. John Nimmo for their guidance, support, and enthusiasm throughout the project. Invaluable field work and guidance were provided by Dave Stonestrom, Jim Constantz, and Fred Gephardt of the U.S. Geological Survey, without whose contributions this project would not have been possible. I also very much appreciate the help and suggestions provided by Kari Winfield, Kim Perkins, Amy Stewart, and Rich Niswonger throughout this project.

TABLE OF CONTENTS

	Page
INTRODUCTION.....	1
FLOW IN THE UNSATURATED ZONE.....	4
PREVIOUS STUDIES.....	8
SITE DESCRIPTION.....	10
METHODS.....	17
Sample Collection.....	17
Sample Analysis.....	21
Soil Property Measurements.....	21
Hydraulic Property Measurements.....	22
RESULTS.....	25
Soil Properties.....	25
Hydraulic Properties.....	29
Soil Moisture Retention.....	29
Unsaturated Hydraulic Conductivity.....	32
Point Recharge Estimates.....	41
Comparison of $K(\theta_f)$ to C_u and D_{10}	42
DISCUSSION.....	45
Depth to Steady Flow.....	45
Channel Recharge.....	46

Terrace Recharge.....	49
Total Recharge Analysis.....	51
Subregion Delineations.....	53
Subregion 1 – Rio Grande active floodplain.....	53
Subregion 2 – Fluvial terraces of the ancestral Rio Grande..	55
Subregion 3 – Piedmont slope.....	55
Effective Channel Width.....	57
Recharge Estimate.....	62
Comparison to Other Studies.....	62
Uncertainty in Upscaling.....	65
Uncertainty in Effective Channel Width	66
CONCLUSIONS.....	67
REFERENCES CITED.....	69

LIST OF ILLUSTRATIONS

Figure		Page
1.	Map of the Middle Rio Grande Basin.....	2
2.	Hypothetical Profile of Matric Pressure.....	6
3.	Site Map of Abo Arroyo.....	11
4a.	Photo of Abo Arroyo near the Basin Margin.....	12
4b.	Photo 12 km Down-Channel from the Basin Margin.....	12
4c.	Photo 28 km Down-Channel from the Basin Margin.....	13
5.	Daily Mean Discharge at Stream Gage	15
6.	Site Map with Borehole Locations.....	18
7a.	Aerial View of Abo Arroyo entering the MRGB.....	19
7b.	Aerial View 12 km Down-Channel from the Basin Margin.....	19
7c.	Aerial View 20 km Down-Channel from the Basin Margin.....	20
7d.	Aerial View 28 km Down-Channel from the Basin Margin.....	20
8a.	Particle Size Distribution for Channel Samples.....	26
8b.	Particle Size Distribution for Terrace Samples.....	26
8c.	Particle Size Distribution for Surface Samples.....	27
9.	Particle Size Histogram for Surface Samples.....	30
10a.	Soil-Moisture Retention Curves for Channel Samples.....	31
10b.	Soil-Moisture Retention Curves for Terrace Samples.....	31
11a.	K(θ) Curves for Channel Samples.....	33

11b.	K(θ) Curves for Terrace Samples.....	33
12a.	K(θ) Curve and K(θ_f) for Sample C1-a and C1-b.....	34
12b.	K(θ) Curve and K(θ_f) for Sample C1-c and C1-d.....	34
12c.	K(θ) Curve and K(θ_f) for Sample C2.....	35
12d.	K(θ) Curve and K(θ_f) for Sample C3-a and C3-b.....	35
12e.	K(θ) Curve and K(θ_f) for Sample C6.....	36
12f.	K(θ) Curve and K(θ_f) for Sample C7.....	36
12g.	K(θ) Curve and K(θ_f) for Sample C8-a and C8-b.....	37
12h.	K(θ) Curve and K(θ_f) for Sample T1.....	38
12i.	K(θ) Curve and K(θ_f) for Sample T2.....	38
12j.	K(θ) Curve and K(θ_f) for Sample T3.....	39
12k.	K(θ) Curve and K(θ_f) for Sample T4.....	39
12l.	K(θ) Curve and K(θ_f) for Sample T5.....	40
13a.	Comparison of C_u and K(θ_f) for Channel Cores.....	43
13b.	Comparison of C_u and K(θ_f) for Terrace Cores.....	43
13c.	Comparison of C_u and K(θ_f) for Surface Samples.....	43
14a.	Comparison of D_{10} and K(θ_f) for Channel Cores.....	44
14b.	Comparison of D_{10} and K(θ_f) for Terrace Cores.....	44
14c.	Comparison of D_{10} and K(θ_f) for Surface Samples.....	44
15.	Variation in Recharge Rate Along Reach of Abo Arroyo.....	47
16.	Comparison of Terrace and Channel Recharge Rates	50

17.	Infiltration Rate as a Function of D_{10}	52
18.	Aerial View of Abo Arroyo and Borehole C8.....	54
19a.	Exponential Fit to Subregion 3 Recharge Estimates.....	58
19b.	Exponential Fit to Subregion 2 and 3 Recharge Estimates.....	58
20.	Diagram Depicting Effective Channel Width.....	60
21.	Subregion Delineations and Recharge Estimates.....	63
22.	Comparison of Total Recharge Estimates.....	64

LIST OF TABLES

Table		Page
1.	Summary of Sampling Dates and Locations.....	17
2.	Summary of Core-Sample Soil Properties.....	25
3.	Effective Particle Diameter and Coefficient of Uniformity.....	28
4.	Summary of Sample Depths, $K(\theta_r)$, and Inferred Recharge Rate....	41
5.	Comparison of Terrace Recharge Rates.....	49
6.	Recharge for each Sub-Region and Total Recharge.....	62

INTRODUCTION

In the arid and semi-arid Southwest, infiltration through ephemeral stream channels can be an important source of ground-water recharge. The Middle Rio Grande Basin (MRGB), located in central New Mexico (Fig. 1), is one such location where infiltration through ephemeral washes likely represents a significant percentage of recharge to the regional aquifers. Approximately half (about 750,000 people) of the total population of New Mexico lives within the MRGB. Recent rapid growth in the basin has placed increasing stress on these aquifers resulting in ground-water withdrawals exceeding recharge (McAda, 1996). Due to dramatic declines in water levels in recent years, a more complete characterization of the ground-water resources in the MRGB has become necessary. The current USGS ground-water flow model for the MRGB (Kernodle and others, 1995) suggests sources and quantities of ground-water recharge, but few direct measurements have been made in these areas. Improved estimation of recharge from these sources, including recharge resulting from infiltration through ephemeral streams, will reduce uncertainties in recharge estimates to the MRGB.

The primary objective of this study is to provide improved knowledge of the spatial distribution of recharge rates at various locations in and adjacent to a 28-km reach of Abo Arroyo, located in the southeast corner of the MRGB. Samples obtained from distinct locations will provide information on variations in recharge rate with distance down-channel, away from the basin margin, and with lateral distance away from the channel. A secondary objective is to evaluate the dependence of recharge rate on the

geologic and hydrologic environment. From this information, total annual recharge through the arroyo will be estimated for comparison to other estimates. Point recharge estimates have been obtained on core-samples collected within the unsaturated zone through application of the steady-state centrifuge (SSC) method.

FLOW IN THE UNSATURATED ZONE

Downward, one-dimensional flow in the unsaturated zone is driven primarily by gravity and matric pressure gradients (matric pressure is a measure of how strongly the water is held by the soil). Whereas gravity drives flow in the downward direction, matric pressure gradients can drive flow in either the downward or upward direction and, in three-dimensions, can drive flow in any direction. Water that moves downward through the unsaturated zone contributes to aquifer recharge, and under appropriate circumstances, a measured vertical flux density (q) below the root zone may be interpreted as a long-term, average recharge rate (Nimmo and others, 1994).

Assuming water is driven downward according to Darcy's law, water fluxes beneath the root zone can be estimated by measurement of unsaturated hydraulic conductivity and potential gradients, e.g., gravity potential and matric potential. Darcy's law, though originally conceived for steady-state saturated flow, was extended by Buckingham (1907) to steady-state unsaturated flow. The Buckingham-Darcy flux law states that fluid flow, or flux (q), is a function of the total driving force ($\partial\Phi/\partial z$) times a constant of proportionality K , the unsaturated hydraulic conductivity as a function of water content (θ):

$$q = -K(\theta)[\partial\Phi/\partial z]$$

with z positive upwards. The total hydraulic potential, Φ , is expressed as:

$$\Phi = \phi_{sw} + \phi_g$$

where ϕ_g is the elevation potential z , and ϕ_{sw} is the soil-water potential. Generally, the major component of ϕ_{sw} is taken to be the matric potential ψ , so that the total potential is the sum of matric potential and elevation potential

$$\Phi = \psi + z$$

Thus,

$$q = -K(\theta)[\partial\psi/\partial z + \partial z/\partial z] = -K(\theta)[\partial\psi/\partial z + 1]$$

where q is the flux density, K is the unsaturated hydraulic conductivity as a function of water content, $\partial\psi/\partial z$ is flow driven by matric pressure gradients, and $\partial z/\partial z = 1$ is downward flow driven by gravity (negative z direction). Whereas gravity is essentially constant everywhere, matric pressure can vary significantly with position in the soil profile. Water will tend to flow from wetter areas of low suction (matric pressure close to zero) to drier areas of high suction (large negative matric pressures). Figure 2 illustrates the ψ profiles that can develop in a thick unsaturated zone. At relatively shallow levels, soil-water content can fluctuate dramatically both in time and position within the soil profile. Infiltration during precipitation and flooding events can greatly increase soil water content at shallow levels, whereas hot dry weather can cause tremendous amounts of evaporation and transpiration. As a result of these spatial and temporal fluctuations in water content, matric potential will fluctuate accordingly, setting up matric potential gradients large enough to affect flow. However, if the unsaturated zone is deep enough, fluctuations may be completely damped at depth so as to create a zone of uniform θ and ψ (Gardner, 1964). Given that ψ is constant with depth, there is

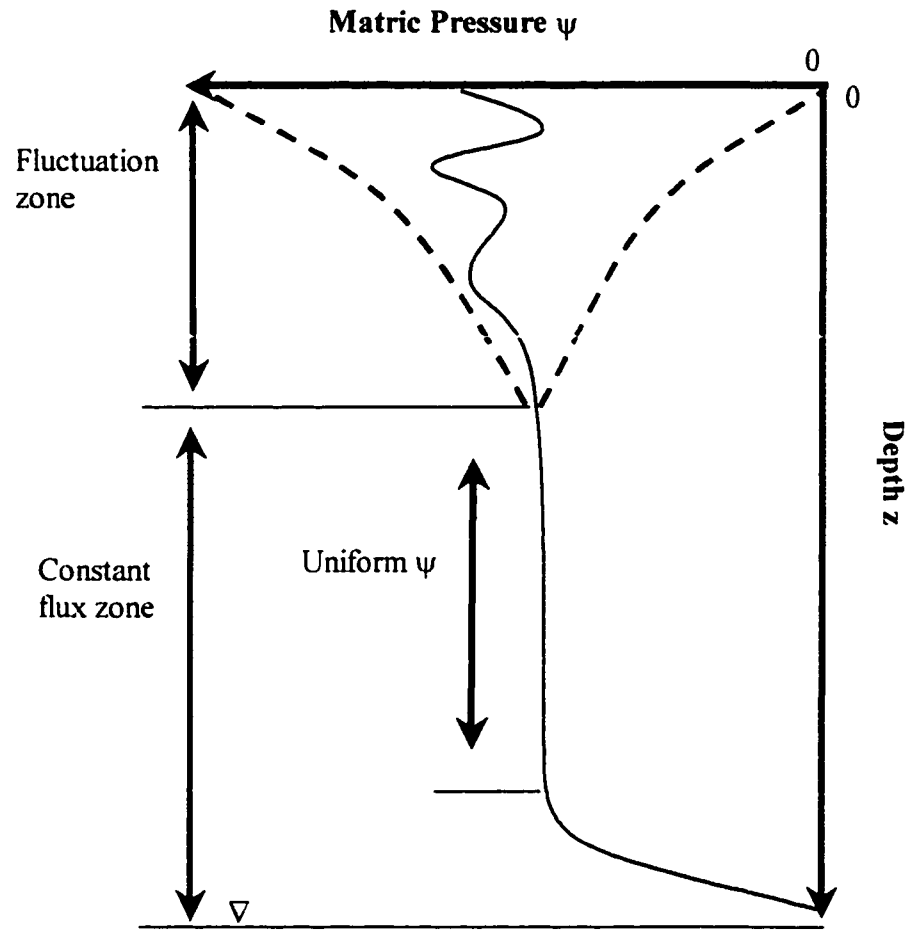


Figure 2. Hypothetical profile of matric pressure as a function of depth in an unsaturated zone deep enough that its lower portion has a constant downward flux (q) of water. Dashed lines represent possible extremes in matric pressure.

no matric potential gradient to drive flow (i.e., if $\psi = \text{constant}$, then $\delta\psi/\delta z = 0$). The result is a zone in which q is also uniform (constant with depth) and steady (constant with time) with gravity driving downward flow (unit gradient flow). Uniform q can exist in layered profiles as well (Nimmo and others, 1994). If the layers are sufficiently thick, uniform- ψ zones can develop within a layer, so that flow is still essentially driven by gravity alone. However, steady state water content will not necessarily be the same for separate layers.

With flow driven by gravity alone, water fluxes beneath the root zone can be determined by measuring K at the in-situ water content of a core sample collected from within the zone of uniform and steady flow ($q = -K(\theta_{\text{in-situ}})$). Also, because the sample is from a depth where q remains constant in time, q can be interpreted as the long-term average recharge rate (R) at the location of the sample.

PREVIOUS STUDIES

Recharge along most tributaries to the Rio Grande, including Abo Arroyo, has been estimated by indirect methods (water-budget methods). These studies generally used long-term average annual precipitation and drainage basin area to obtain average annual recharge through an arroyo. Kernodle and Scott (1986), Hearne and Dewey (1988), and Waltermeyer (1994) have each estimated average annual recharge through Abo Arroyo using empirically derived rainfall/ watershed area equations. Results range from 4,220 to 40,600 acre-ft/yr. Scott Anderholm has more recently estimated recharge through Abo Arroyo (Anderholm, in press) at roughly 900 acre-ft/yr.

Two other studies have recently been undertaken to obtain point recharge estimates within and adjacent to Abo Arroyo. Dave Stonestrom has employed a chloride-mass-balance (CMB) technique to obtain recharge estimates at point locations outside the arroyo channel, on the adjacent inter-arroyo region (denoted arroyo terraces in this study). Results indicate that recharge rates range from 0.04 to 2 mm/yr on the arroyo terraces (Stonestrom and Akstin, 1998). Jim Constantz and others are using a thermal-pulse tracking technique to obtain recharge rate estimates at specific locations within Abo Arroyo. As of October 2000, no recharge estimates using thermal pulse tracking have been published.

Results using the SSC method as a technique for estimating recharge rates at other sites have been published by Nimmo and others (1994). The SSC method was applied to two distinct hydrogeologic settings, one an alluvial fan in the San Joaquin Valley of

California, and the other a loess deposit in Washington state. Reliable recharge estimates for the San Joaquin Valley site could not be determined due to uncertainty in matric pressure gradient, however reasonable recharge estimates were obtained for the Washington site, demonstrating the viability of the SSC method as a technique for estimating recharge under appropriate conditions.

SITE DESCRIPTION

Abo Arroyo, located about 70 km southeast of Albuquerque, flows west through a gap between the southern Manzano and the northern Los Pinos Mountains and out onto the MRGB for approximately 29 km where it meets the Rio Grande (Fig. 3). West of the mountain front, Abo Arroyo cuts into a large Pleistocene fan (the Abo Canyon fan) deposited downstream from Abo Arroyo Canyon located in the southern Manzano Mountains. Below the distal portion of the fan, roughly 12 km down-channel, Abo Arroyo cuts into a stepped sequence of four fluvial terraces that represent episodes of valley cutting by the Rio Grande during the late Pleistocene (Titus, 1963). Beyond the abandoned fluvial terraces, approximately 27 km down-channel, Abo Arroyo cuts across the active flood plain of the Rio Grande for approximately 1 km before entering a flood control channel leading to the Rio Grande.

Sediments within the upper portions of Abo Arroyo are late Quaternary alluvium derived from the nearby Manzano and Los Pinos Mountains, whereas sediments in the lower portions of the arroyo contain both Manzano-derived and Los Pinos-derived sediments and reworked sediments of the abandoned Rio Grande fluvial terraces (Hawley and others, 1982). Sediment sizes range from cobble-size or larger in the upper reach of Abo Arroyo to primarily sand-size in the lower reach, near the confluence with the Rio Grande. In addition, sediments display a broad range of particle sizes in the upper reach, ranging from silt-size to cobble-size, whereas down-channel sediment size is more uniform. Figures 4 a, b and c are photographs of Abo Arroyo taken at the upper reach

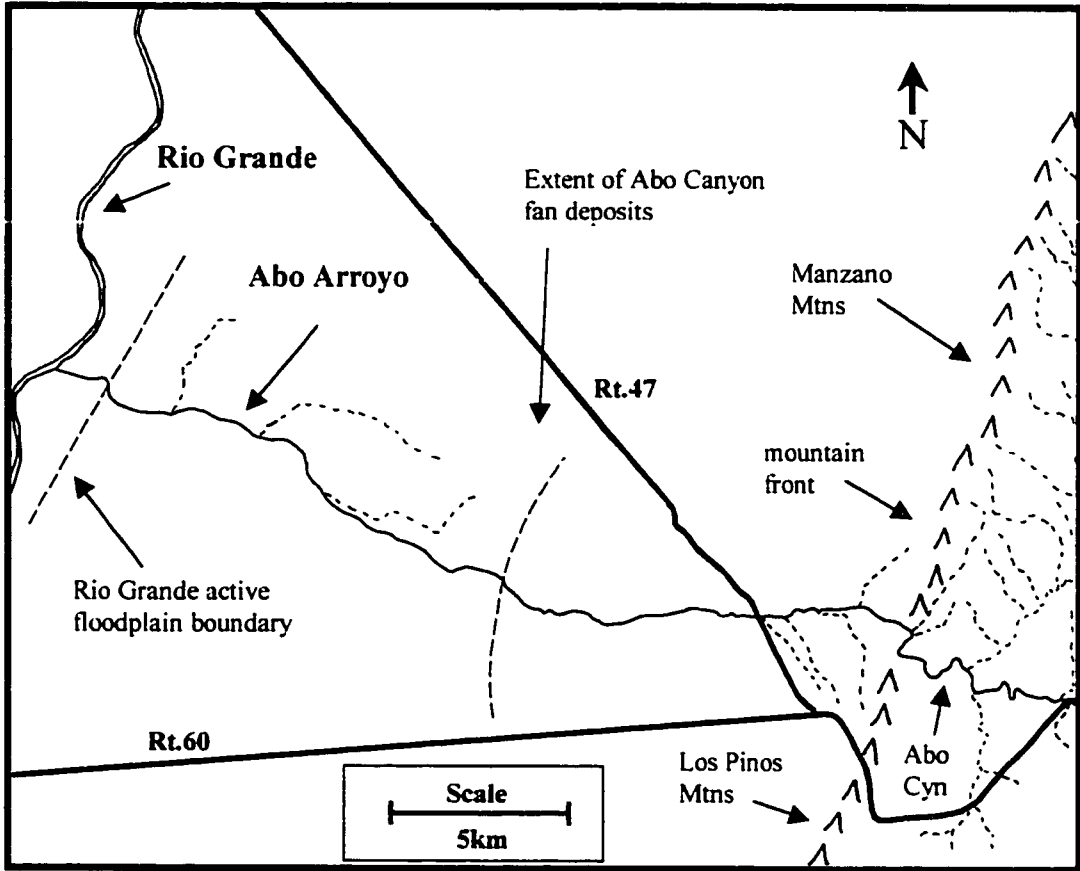


Figure 3. Site map showing close-up of Abo Arroyo and relevant physiographic features.

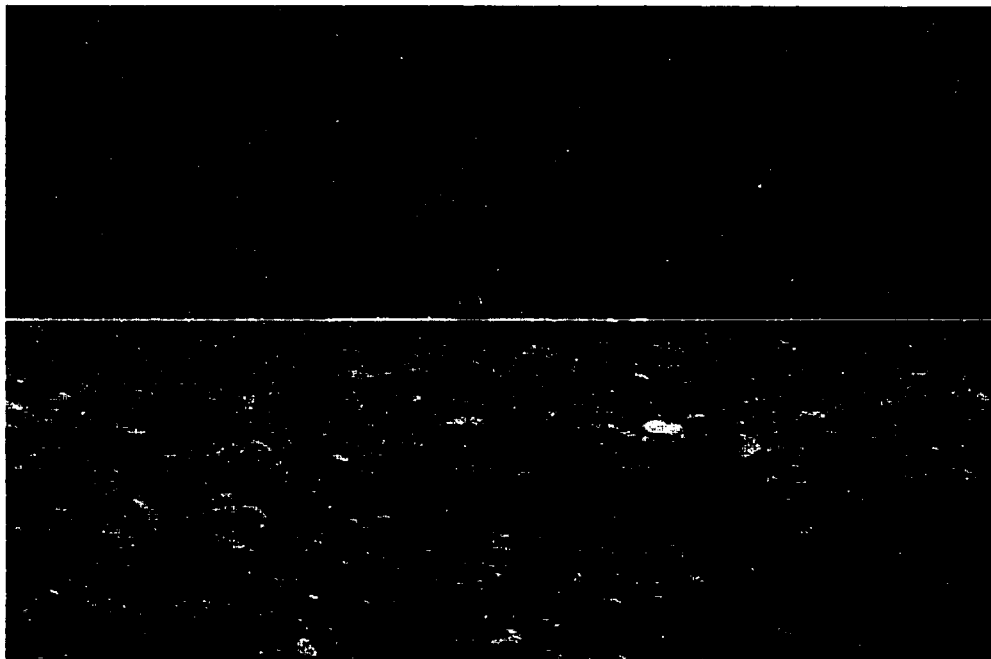


Figure 4a. Photo taken at the upper reach of Abo Arroyo near the basin margin, looking east. Note vehicle in center of photo for scale.

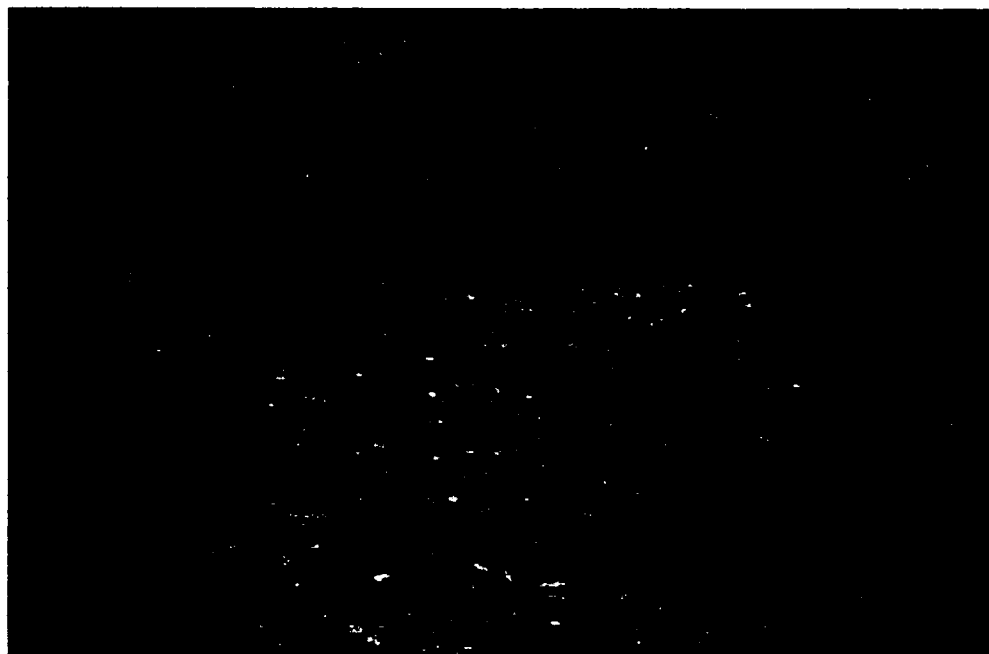


Figure 4b. Photo taken approximately 12 km down-channel from the basin margin, looking west. Arroyo is incised approximately 3 to 4 m at this location.



Figure 4c. Photo of Abo Arroyo taken approximately 28 km down-channel from the basin margin, near the confluence with the Rio Grande. Channel here is approximately 10 m wide.

near the basin margin, 12 km down-channel from the basin margin, and roughly 28 km down-channel near the confluence with the Rio Grande, illustrating the differences in sediment size and size range at different locations along the reach.

The southeastern portion of the MRGB has a semi-arid to arid climate with annual potential evaporation (~140 cm/yr) greatly exceeding annual precipitation (~25 cm/yr) (Thorn and others, 1993). Most of the precipitation falls as rain in the summer months, though some falls as winter snow, particularly at the higher elevations of the Manzano and Los Pinos Mountains. Precipitation generally is less than 30 cm/yr in the lowland areas of the southern MRGB, but can exceed 60 cm/yr in the basin bounding mountains. Most runoff into Abo Arroyo occurs in the summer as a result of precipitation in these upland areas. However, in addition to summer runoff, snow melt in these upland areas can produce flows in Abo Arroyo at other times of the year.

Little is known regarding the size, duration, and frequency of flow events through Abo Arroyo. Approximately 2 km up-channel from the basin margin there is a small amount of perennial flow through Abo Arroyo as it cuts across the bedrock of the Manzano Mountains. Below this point, where flow becomes intermittent to ephemeral, the arroyo crosses into a small sub-basin of unconsolidated sediments before entering the MRGB. A stream flow gaging station, located where there is perennial flow, has been operating since August 1996. Stream gage data (Fig. 5) indicate that the small perennial flow is supplemented with multiple short-duration large flow events during the summer. Individual flow events mostly do not last more than 4 to 6 hours (Jim Constantz, Scott Anderholm, 1998 pers. comm.), and the down-channel extent of these flows, including

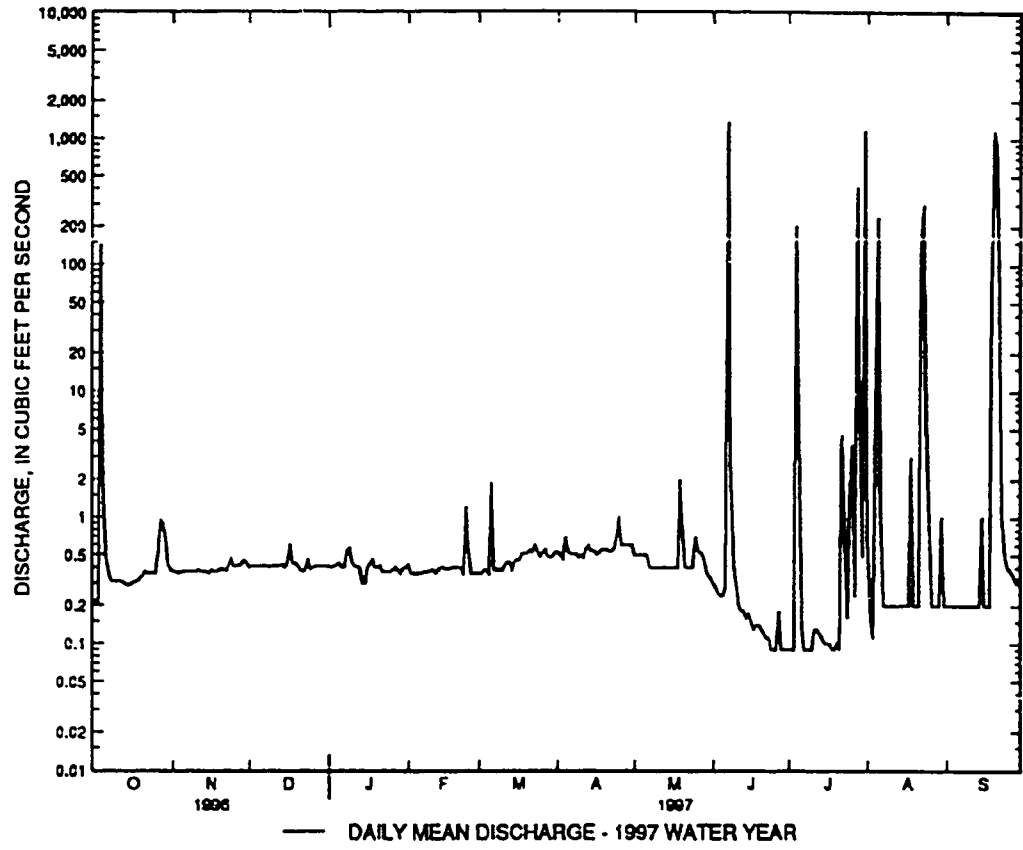


Figure 5. Daily Mean Discharge at stream gage located in Abo Arroyo, 1.5 km up-channel from the basin margin.

whether or not they reach the Rio Grande and their contribution to aquifer recharge, is not well known.

The unsaturated zone beneath Abo Arroyo is 30 to 120 m (100 to 400 ft) thick at the basin margin, in part attributable to faulting, and 5 to 30 m (15 to 100 ft) thick near the confluence with the Rio Grande (Titus, 1963).

METHODS

Sample Collection

Core samples were collected in August 1996, April-May 1997, and June 1998 to depths of 5.4 m at various locations in and adjacent to the study reach of Abo Arroyo. Six locations were sampled in the main channel of Abo Arroyo, and 5 separate locations were sampled 3.5 to 465 m away from the channel (Table 1, Fig. 6). Figures 7a, b, c, and d show aerial views of sample locations.

Table 1: Summary of sampling dates and locations.

Channel samples			
Sample id	Date drilled	Distance from mountain front (km)	Depth (m)
C1-a	8/15/96	1.4 km (up-channel)	0.4 m
C1-b	8/15/96	1.4 km (up-channel)	0.5 m
C1-c	8/15/96	1.4 km (up-channel)	1.9 m
C1-d	8/15/96	1.4 km (up-channel)	2.0 m
C2	8/15/96	0.3 km	2.6 m
C3-a	4/28/97	0.4 km	4.0 m
C3-b	4/28/97	0.4 km	4.2 m
C6	6/21/98	12 km	2.3 m
C7	6/21/98	20 km	2.3 m
C8-a	5/1/97	28 km	5.2 m
C8-b	5/1/97	28 km	5.4 m

Terrace Samples				
Sample id	Date drilled	Distance from mountain front	Distance from arroyo	Depth
T1	8/13/96	1.4 km (up-channel)	5 m	4.6 m
T2	8/13/96	1.4 km (up-channel)	65 m	5.4 m
T3	4/29/97	0.4 km	3.5 m	5.5 m
T4	4/30/97	5 km	5 m	5.4 m
T5	5/2/97	5 km	465 m	5.4 m

Core samples for use in the centrifuge were collected in 1.075-inch diameter brass liners through the use of a Geoprobe (Stonestrom and Akstin, 1998) which is able to

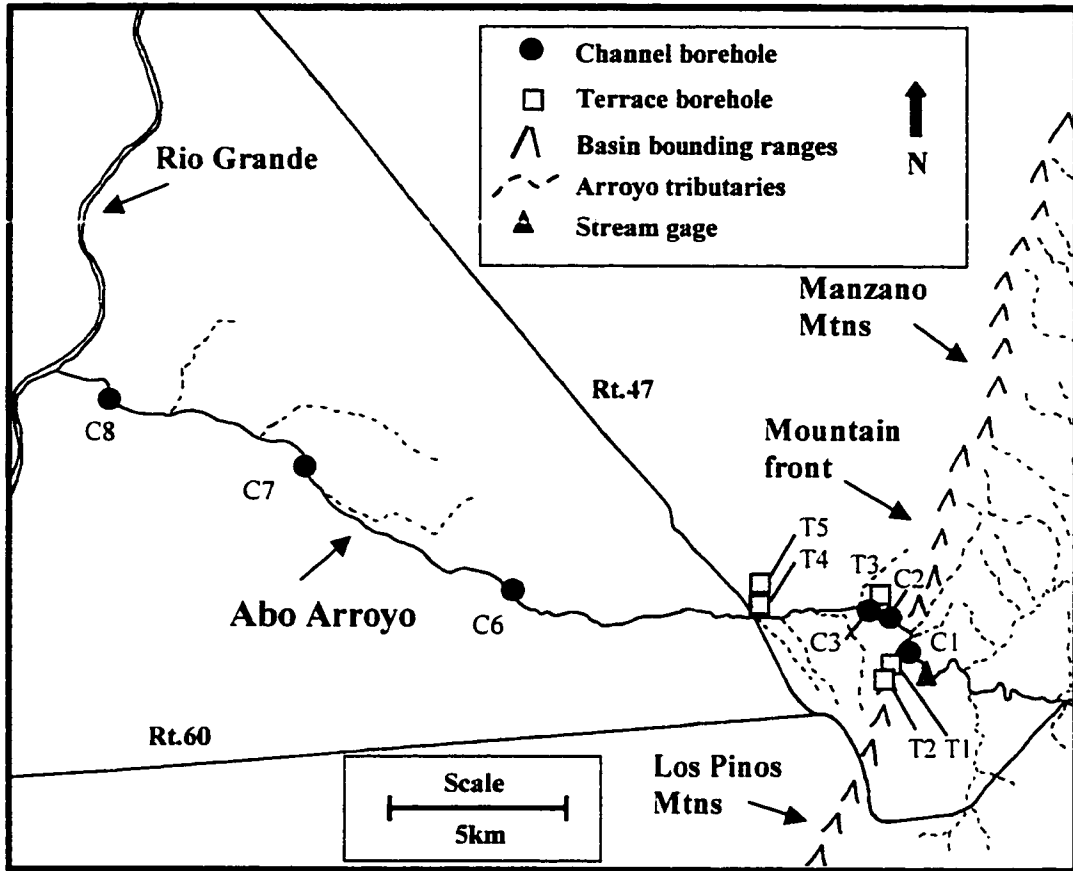


Figure 6. Site map with borehole locations and stream gage location.

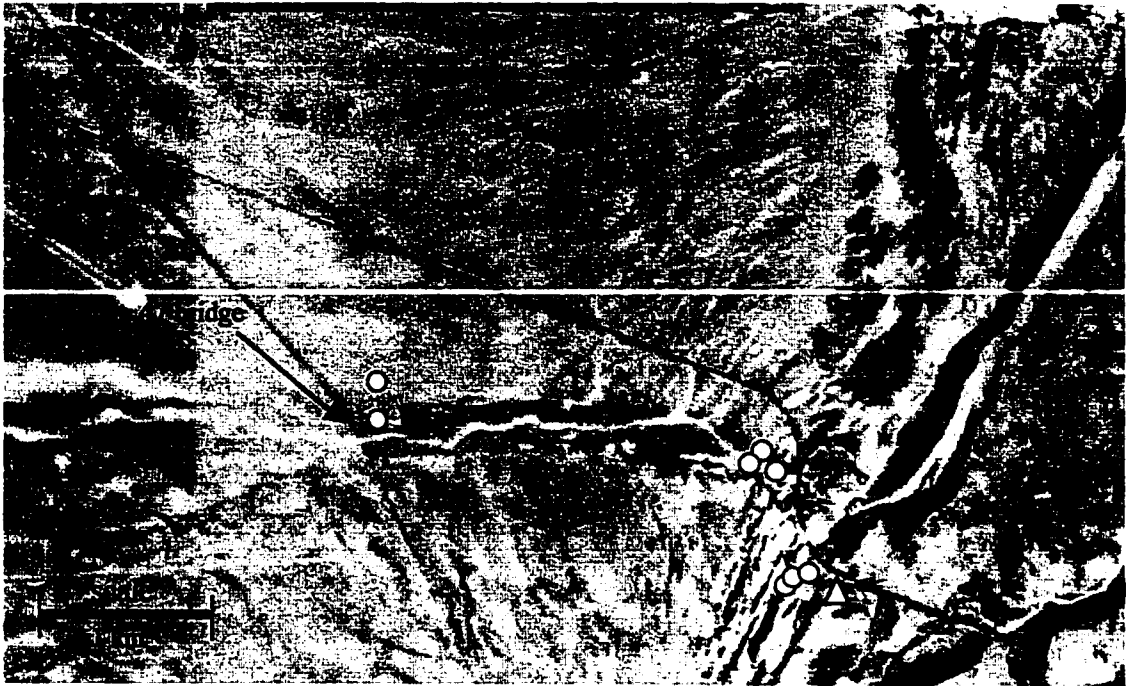


Figure 7a. Aerial view of Abo Arroyo entering the MRGB from the Manzano Mountains with approximate location of boreholes (circles) and stream gage (triangle).

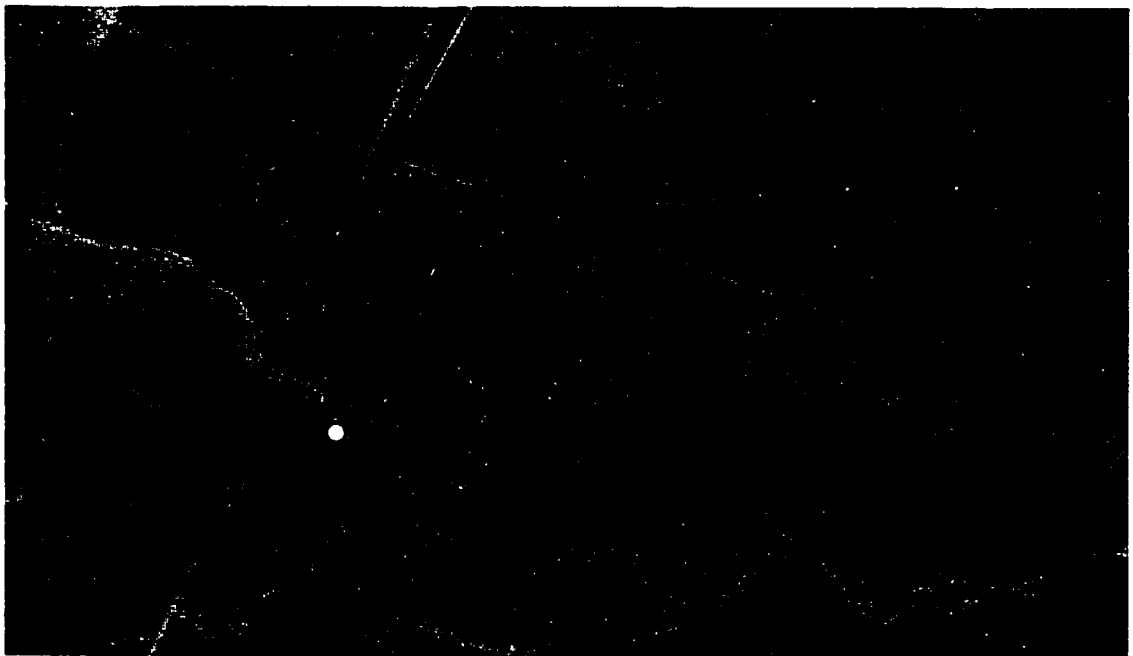


Figure 7b. Aerial view of borehole C6, roughly 12 km down-channel from the basin margin.

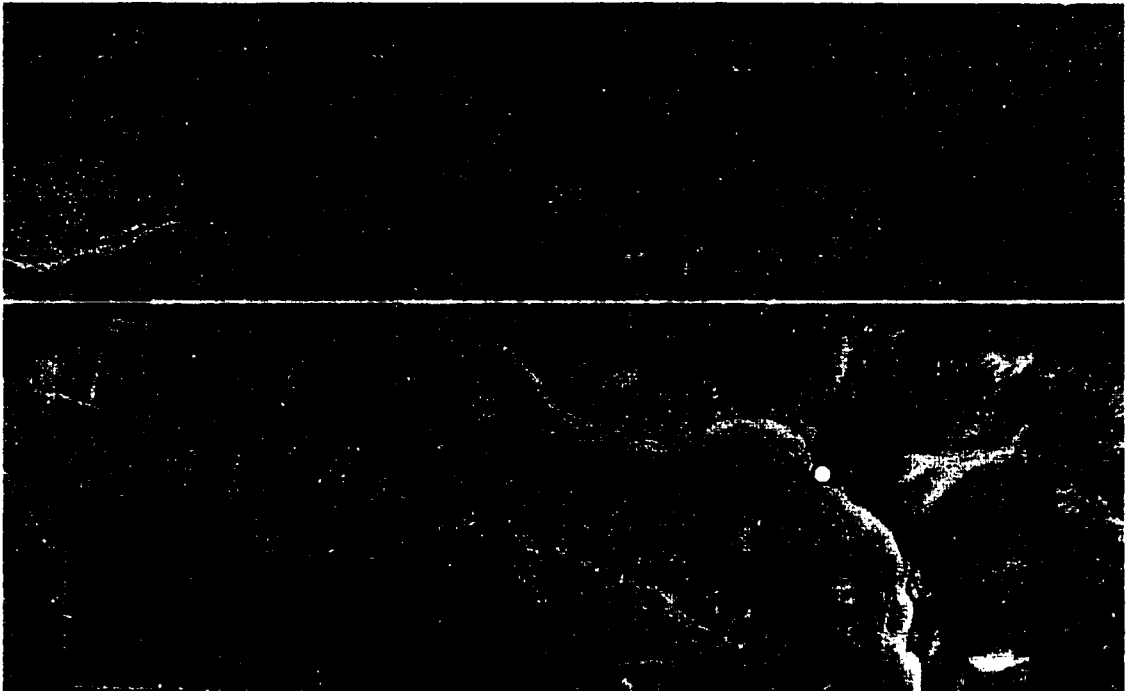


Figure 7c. Aerial view of area around borehole C7, 20 km down-channel from basin margin.



Figure 7d. Aerial view of borehole C8, near the confluence of Abo Arroyo and the Rio Grande (upper left of photo), 28 km down-channel from basin margin.

mechanically extract cores with minimal disturbance. Once extracted, the samples were sealed in order to preserve field water content, later to be measured in the lab.

Additional fieldwork included collection of surface sediment samples (denominated "Abo" in sample identification) at 5 locations within Abo Arroyo. Samples were collected by scooping the sediment directly into 1-liter sample containers. In order to obtain a representative sample from each channel location, five samples were collected at each of the 5 channel locations. The samples were collected in a five-node cross-pattern, with each end-node spaced 1 meter away from the central node. Surface sample location numbers coincide with channel borehole location numbers (e.g. Abo 8 was collected at the location of C8) except Abo 3, which was collected approximately 10 m down-channel from sample location C3, and Abo 4, which was collected approximately 2 km down-channel from sample location C3. Active channel width was also measured at each sample location for use in estimating total recharge through the arroyo.

Sample Analysis

Soil Property Measurements

Following hydraulic property measurements, core samples were oven-dried at 105 °C. Core sample volume and dry weight were measured to obtain bulk density (ρ_b). Particle density (ρ_p) was measured with a pycnometer (Blake and Hartge, 1986), and porosity was calculated from the measured particle and bulk densities.

Particle size distributions were obtained for samples using sieves and a Coulter optical (laser-scattering) particle size analyzer. The entire core sample (30 to 60 grams

dry weight) was sieved for particle sizes larger than 750 μm . The remaining fraction (< 750 μm) was split until a 0.5 to 3 g sample was obtained for optical particle size analysis (750 to 0.04 μm).

Hydraulic Property Measurements

Recharge rate estimates were determined using the steady state centrifuge (SSC) method described by Nimmo and others (1994). This technique involves measurements of unsaturated hydraulic conductivity (K), matric pressure, and water content, and application of Darcy's law to compute fluxes. The SSC technique is well suited for this study because it provides accurate K measurement at low water contents, typical of the desert Southwest.

The SSC technique requires application of water at a constant rate to the core sample through use of a precision pump, and a driving force applied by an appropriate centrifuge speed. The experiment is run at several different flow rates and centrifuge speeds to measure unsaturated K over a range of steady-state water contents that includes or comes as close as possible to the field water content of the sample. In addition, after a centrifuge run, the matric pressure associated with steady-state water content is measured by placing the sample in contact with a tensiometer. Using Darcy's law and measured unsaturated K, downward flux density (q) can be computed.

Steady-state fluid flow in the centrifuge is governed by an equation similar to the equation for steady flow in the unsaturated zone, but with centrifugal force replacing

gravity as a driving force. And in the case of flow in a centrifugal field, matric potential varies as a function of radial distance from the center of rotation rather than depth:

$$q = -K(\theta)[\partial\psi/\partial r - C\rho\omega^2 r]$$

with

C: unit conversion factor of 1 cm-water/980.7 dyne/cm² (i.e., 1 cm of water is equivalent to 980.7 dyne/cm² of pressure),

ρ : density of the fluid passing through the medium (taken to be 1 g/cm³ for water),

ω : angular velocity (rad/s = 1/s since radians are dimensionless).

r: radial distance from the center rotation (cm).

The driving force is applied by choosing a centrifuge rotation speed large enough that the net driving force ($\partial\psi/\partial r - C\rho\omega^2 r$) is significantly different from zero, i.e., any matric potential gradients that develop in the core sample during centrifugation are not great enough to cancel out the centrifugal force.

A stricter criterion, which leads to convenience in calculations, is that $\partial\psi/\partial r \ll C\rho\omega^2 r$, for which the flow is essentially driven by centrifugal force alone. The flow equation then simplifies to:

$$q = -K(\theta)[C\rho\omega^2 r].$$

Given that the driving force ($\rho\omega^2 r$) is specified by the chosen centrifuge speed, and the flux density ($q = Q/A$) is specified by setting the flow rate (Q) into the sample of known

cross sectional area (A), under these conditions the unsaturated hydraulic conductivity, $K(\theta)$, can be computed without measuring $\partial\psi/\partial r$:

$$K(\theta) = q / (C\rho\omega^2 r).$$

For each centrifuge run for this study, the development of potentially significant matric potential gradients was evaluated through the use of a numerical model (John Nimmo, U.S. Geological Survey). The model uses measured hydraulic properties (θ , ψ , and K_{sat}), flow rate (q), and centrifuge speed ($\omega^2 r$) to estimate $\partial\psi/\partial r$ within the core sample for each centrifuge run. If the matric potential gradient is significant for a particular centrifuge run, $K(\theta)$ is re-calculated using the estimated $\partial\psi/\partial r$ as part of the driving force. These calculations are iterated until the ψ gradients are consistent with the inferred $K(\theta)$.

Before centrifugation, core sample volume and weight were measured for later (after oven-drying) computation of the volumetric field water content (θ_f). After centrifugation, saturated hydraulic conductivity (K_{sat}) was measured using a falling-head bench-top method (Klute and Dirksen, 1986), providing a more complete data set for relating hydraulic conductivity to water content, as well for use in the numerical modeling.

RESULTS

Soil Properties

For each core sample, a comprehensive listing of the measured soil properties, saturated K, and field water content is presented in Table 2.

Table 2. Summary of core-sample soil properties, field water content, and K_{sat} .

Sample	Bulk density	Particle density	Porosity	Field Water content	K_{sat}
C1-a	1.90	2.71	0.2989	0.1744	NM
C1-b	2.17	2.66	0.1848	0.1313	3.60E-05
C1-c	1.85	2.63	0.2978	0.2441	5.30E-04*
C1-d	2.03	2.67	0.2397	0.1757	5.30E-04
C2	1.85	2.65*	0.3021	0.1923	2.29E-04
C3-a	1.86	2.65*	0.2982	0.2052	6.96E-05*
C3-b	1.94	2.70	0.2831	0.1525	6.96E-05
C6	1.81	2.64	0.3151	0.3095	6.77E-05
C7	1.91	2.65	0.2806	0.0726	1.27E-03
C8-a	1.89	2.65*	0.2868	0.1653	1.17E-03
C8-b	1.80	2.64	0.3182	0.1517	1.41E-03
T1	1.82	2.65	0.3133	0.0783	5.73E-06
T2	1.26	2.70	0.5330	0.0660	1.16E-04
T3	1.61	2.65*	0.3920	0.0632	1.22E-04
T4	1.78	2.66	0.3319	0.0283	NM
T5	1.43	2.59	0.4467	0.1866	<5E-06*

* = Estimated
 NM = Not Measured

Terrace and channel core samples, except for C1-a and C1-b, and all surface sediment samples were analyzed for particle size distribution (Fig. 8a, b, and c). Core samples C1-a and C1-b ultimately did not provide a reliable recharge estimate and were therefore not analyzed for particle size distribution. Table 3 displays the effective particle diameter (D_{10}) and the coefficient of uniformity ($C_u = D_{60}/D_{10}$) for surface and core samples. D_{10} represents the grain diameter for which 10% of the sample is finer and D_{60} represents the grain diameter for which 60% of the sample is finer. Cumulative

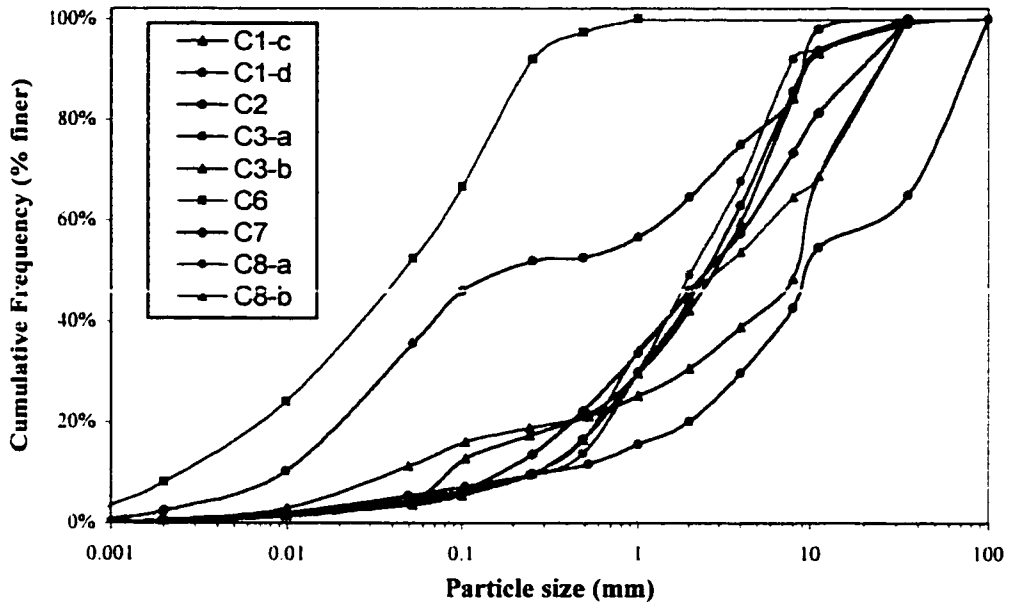


Figure 8a. Particle size distribution for channel samples.

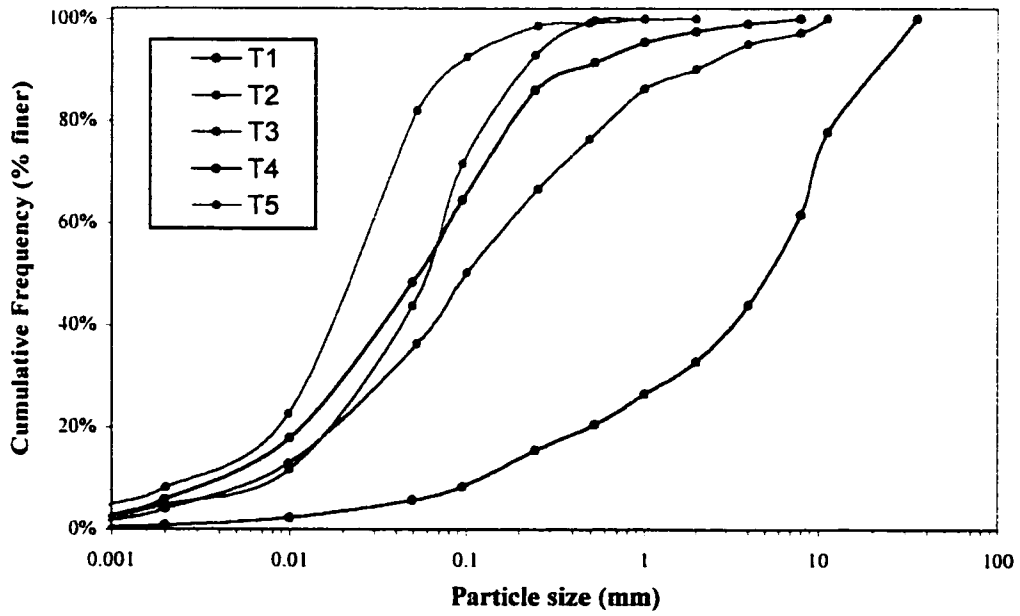


Figure 8b. Particle size distribution for terrace samples.

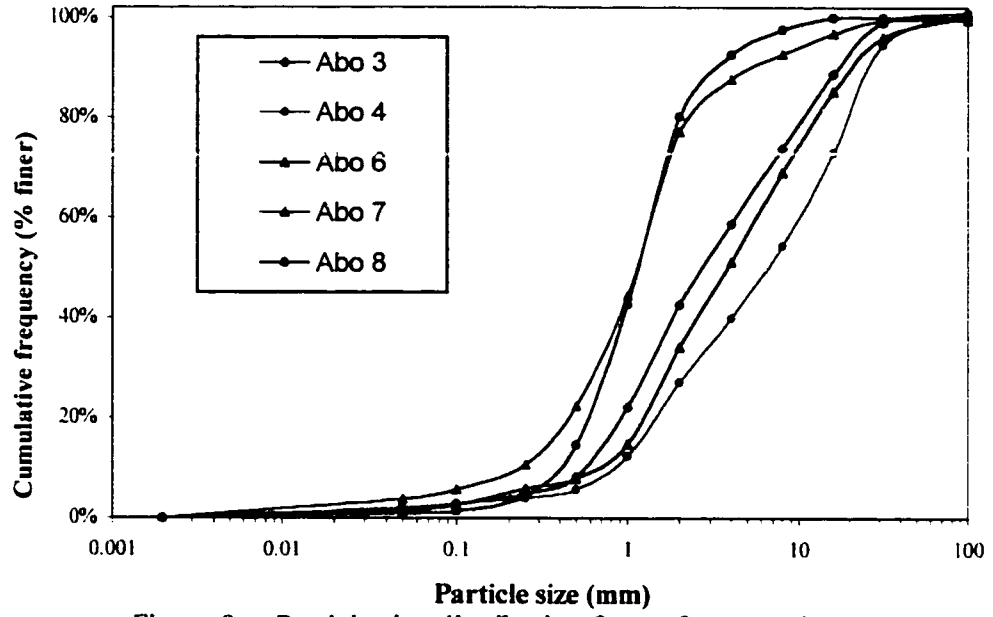


Figure 8c. Particle size distribution for surface samples.

Table 3. Effective particle diameter (D_{10}), D_{60} , and coefficient of uniformity (C_u).

Sample	D_{10} (mm)	D_{60} (mm)	C_u
Abo 3	0.56	4.2	7.5
Abo 4	0.82	10	12
Abo 6	0.66	5.7	8.6
Abo 7	0.24	1.4	5.8
Abo 8	0.42	1.4	3.3
C1-c	0.083	9.4	110
C1-d	0.29	11	39
C2	0.26	3.5	13
C3-a	0.0093	1.4	150
C3-b	0.042	4.1	98
C6	0.0026	0.075	29
C7	0.18	5.0	28
C8-a	0.26	3.0	12
C8-b	0.27	6.3	23
T1	0.0034	0.070	21
T2	0.0078	0.18	22
T3	0.0068	0.076	11
T4	0.14	7.6	54
T5	0.0029	0.031	11

frequency curves and effective particle diameters demonstrate that terrace samples are generally much finer textured than channel surface or channel core samples, consistent with field and laboratory observations. Channel surface and channel core sediment samples generally display a similar range of particle sizes, however, on average, channel surface samples have a larger effective particle diameter. Cumulative frequency curves and effective particle diameters also show that surface sediment size does not necessarily match core sediment size for samples taken at the same location in the channel. Channel surface samples have the highest degree of sorting (small C_u number), channel core samples are very poorly sorted (large C_u number), and terrace samples fall in between. Note that differing sampling techniques (i.e., the size of the sampling container and the

number of sample points as discussed above) for core samples and surface samples may have influenced particle size distribution results.

Regarding surface samples only, samples from the upper reach of Abo Arroyo (Abo 3, 4, and 6) consistently display a greater effective particle size and poorer sorting than surface samples from regions further down-channel (Abo 7 and 8), consistent with field observations. A particle size histogram of surface sediment (Fig. 9) clearly shows that surface sediment samples from the upper reach of Abo Arroyo are coarser, and display somewhat of a bimodal distribution. In contrast, down-channel surface sediment is finer textured and better sorted.

Hydraulic Properties

Soil Moisture Retention

Soil-moisture retention curves are plotted in Figures 10a and b. These curves represent measured and modeled (Brooks and Corey, 1964) matric pressure as a function of measured water content for each centrifuge run. Modeled points are denoted with open symbols, measured points are shaded. Retention curves for channel samples generally have less negative air entry values and a steeper drainage curve, typical of relatively coarse sediments. In contrast, retention curves for terrace samples have higher water content for a given matric pressure and more negative air entry values, typical of finer textured material.

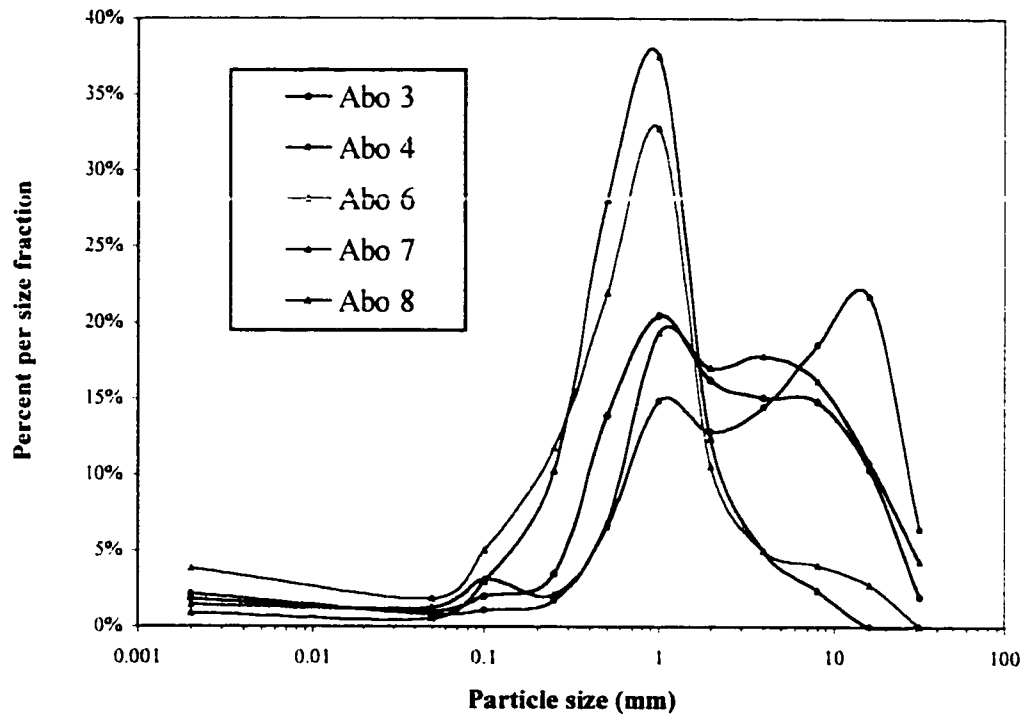


Figure 9. Particle size histogram for surface samples.

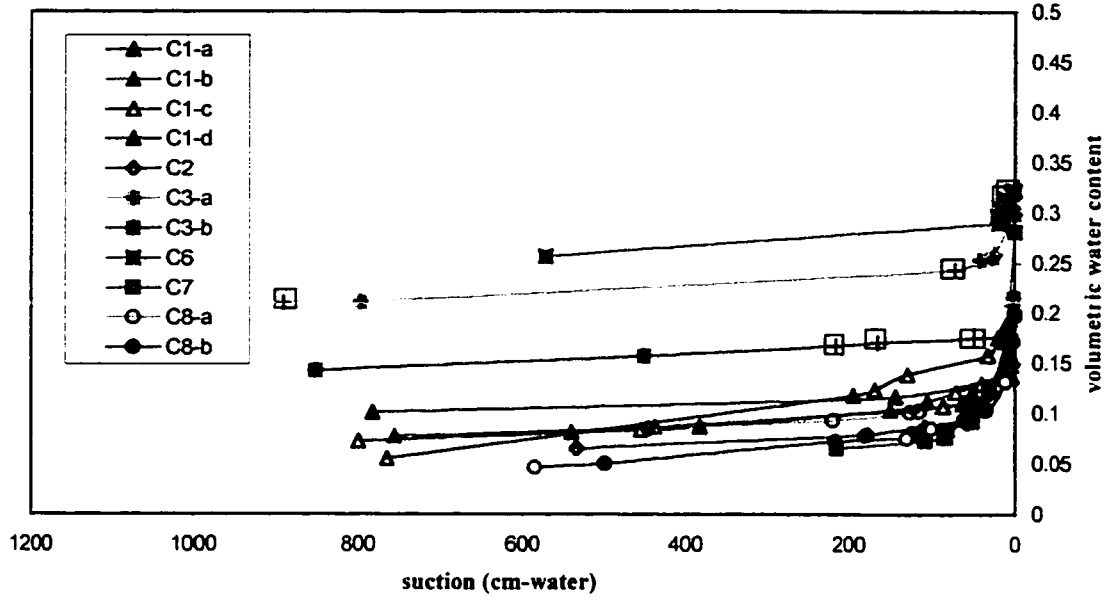


Figure 10a. Soil-moisture retention curves for the channel samples. Shaded points represent measured values, open points are modeled values.

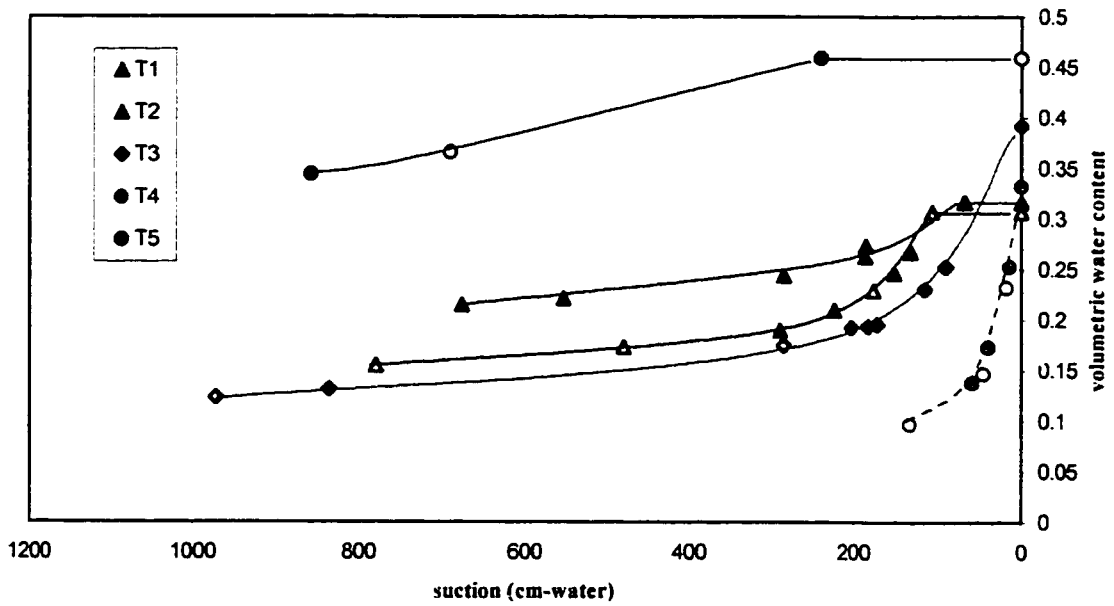
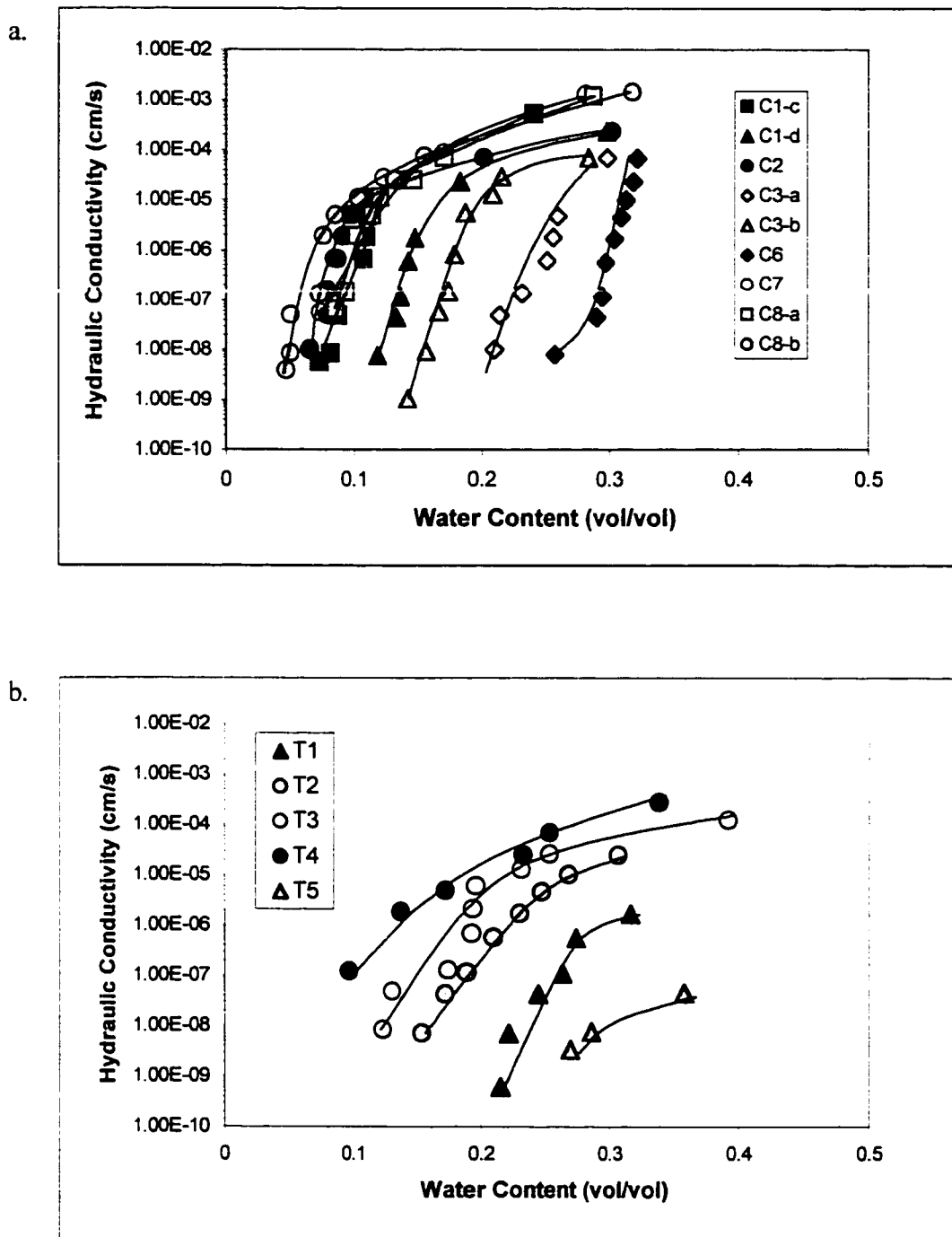


Figure 10b. Soil-moisture retention curves for the terrace samples. Shaded points represent measured values, open points are modeled values.

Unsaturated Hydraulic Conductivity

Figures 11a and b illustrate $K(\theta)$ curves determined for channel and terrace core samples, shown at the same scales for comparison (note that $K(\theta)$ curves for channel samples C1-a and C1-b, samples not used in recharge rate estimates, have been omitted from figure 11a for graphical clarity). Compared to terrace sample K curves, channel sample curves are steeper and generally shifted to lower water content for a given K (i.e. to the left), consistent with coarser textured sediments. In addition, several of the channel samples are located on the same area of the graph with very similar curve shape suggesting strong similarities in their hydraulic properties.

Figures 12a through 12l show $K(\theta)$ curves for channel and terrace core samples grouped by location. Each graph also shows the associated field water content (θ_f) for each sample, and the determined unsaturated K at the field water content $K(\theta_f)$. $K(\theta_f)$ values for channel samples range from 3.9×10^{-09} to 1.0×10^{-04} cm/s whereas $K(\theta_f)$ values for terrace samples are all 4.5×10^{-10} cm/s or less. However, because the field water content of the terrace samples is generally lower than what can be achieved in the centrifuge $K(\theta)$ measurements, the $K(\theta_f)$ values had to be extrapolated rather than interpolated from the K curves. As a result, confidence in the accuracy of terrace recharge rate estimates is diminished. In addition, terrace samples T1 and T3 did not show a clear trend for extrapolating the curve. Therefore, two curves are shown for each of the samples (Fig. 12h and 12j, respectively). One curve (dashed line) represents a trend that leads to a minimum extrapolated $K(\theta_f)$ estimate and the other curve (solid line) represents



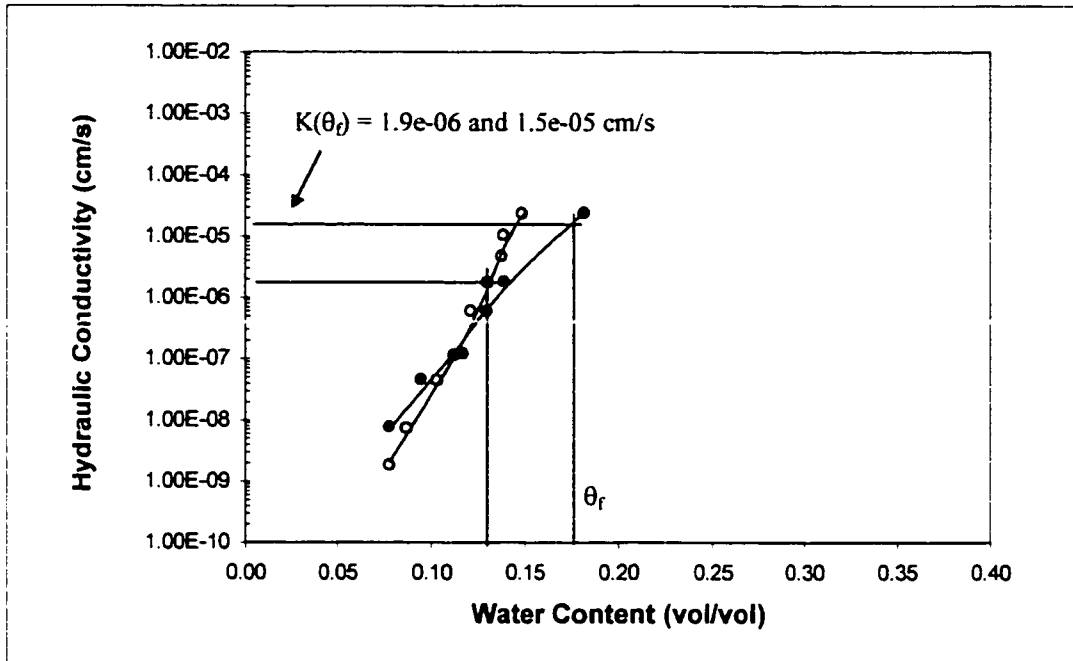


Figure 12a. $K(\theta)$ curve and $K(\theta_f)$ for sample C1-a (closed circles) and C1-b (open circles).

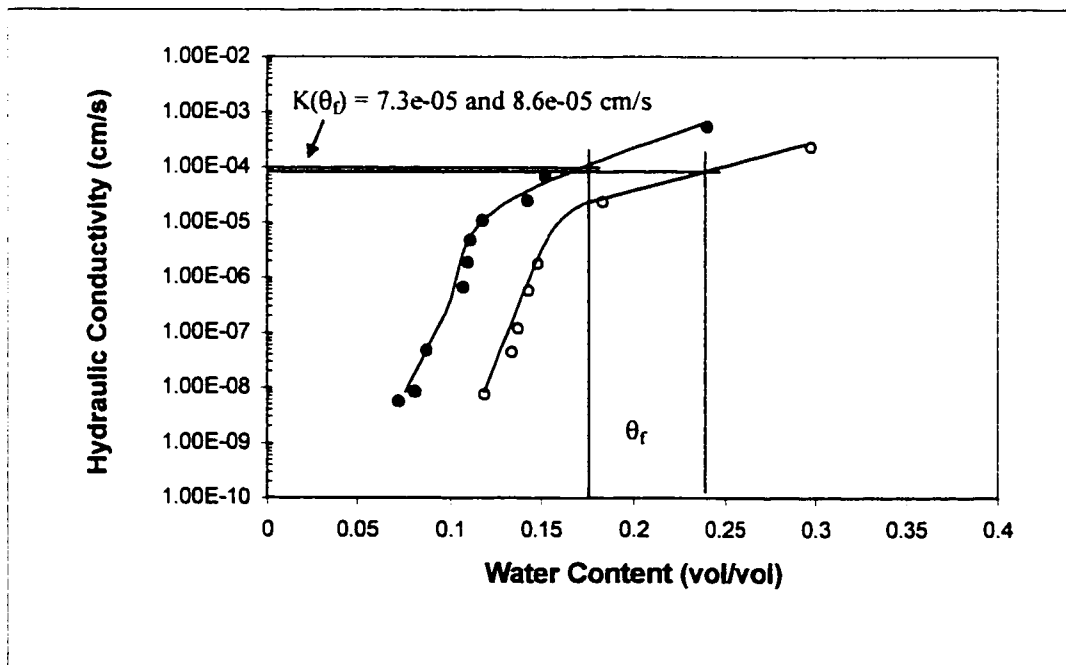


Figure 12b. $K(\theta)$ curve and $K(\theta_f)$ for sample C1-c (open circles) and C1-d (closed circles).

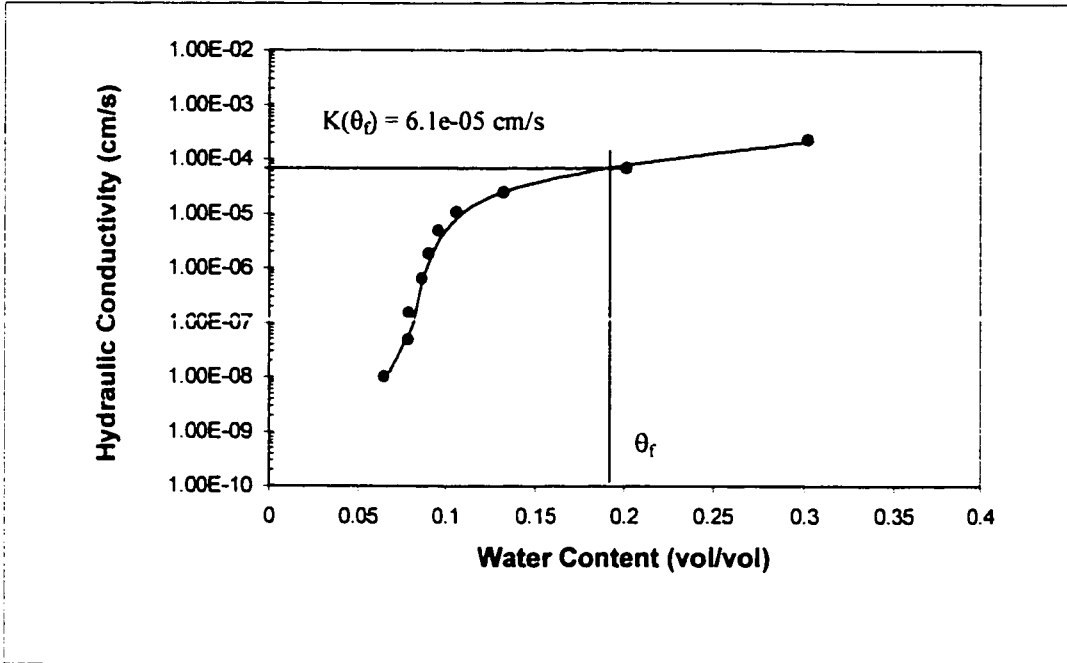


Figure 12c. $K(\theta)$ curve and $K(\theta_r)$ for sample C2.

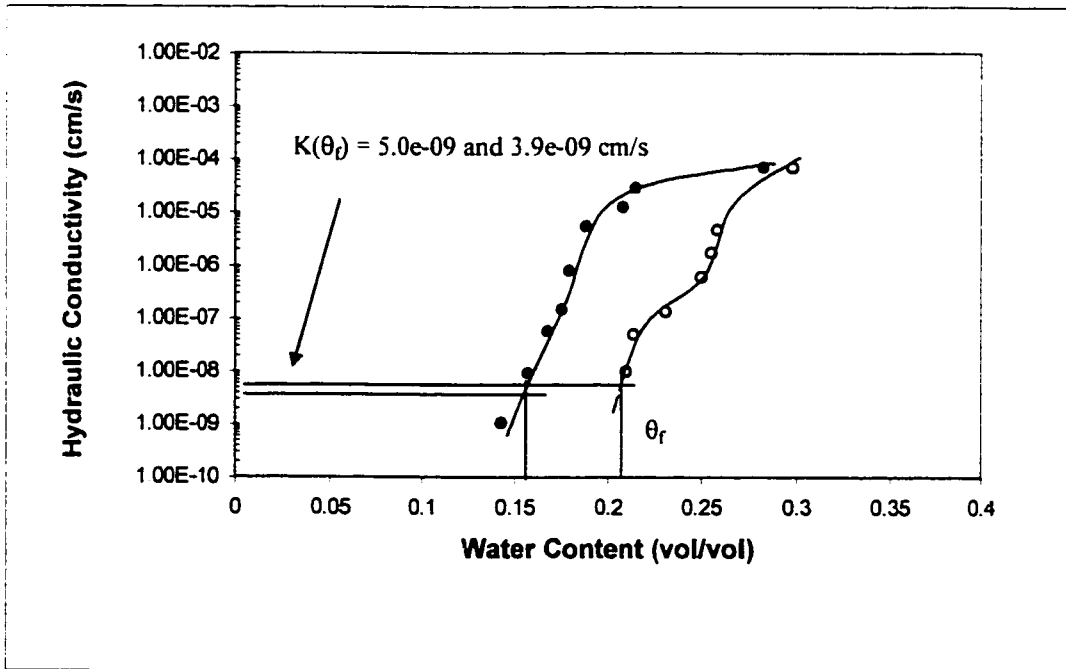


Figure 12d. $K(\theta)$ curve and $K(\theta_r)$ for sample C3-a (open circles) and C3-b (closed circles).

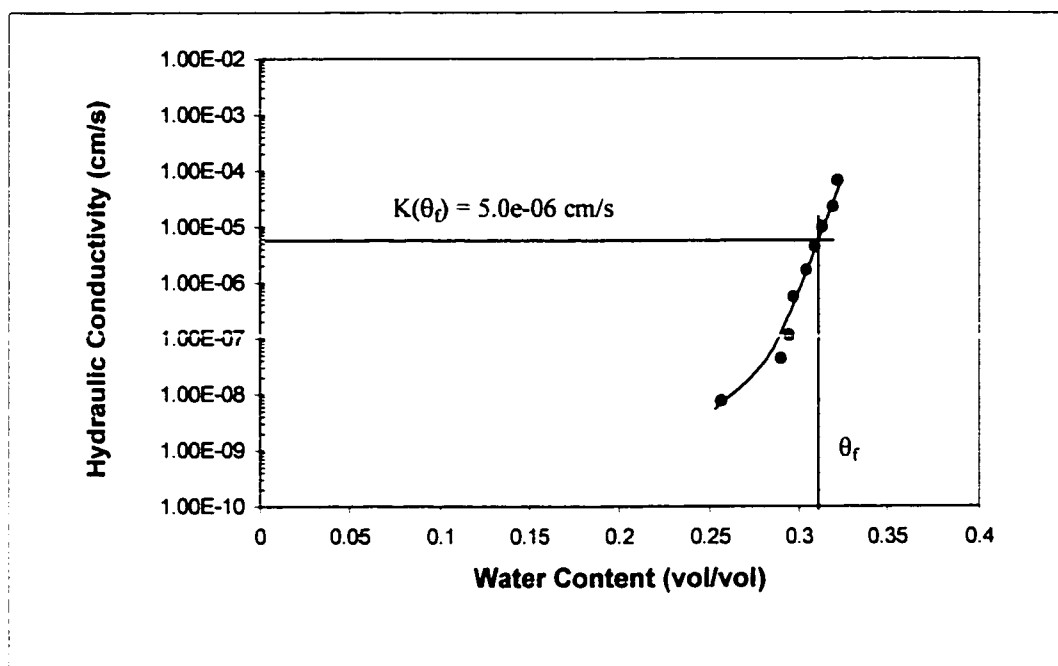


Figure 12e. $K(\theta)$ curve and $K(\theta_f)$ for sample C6.

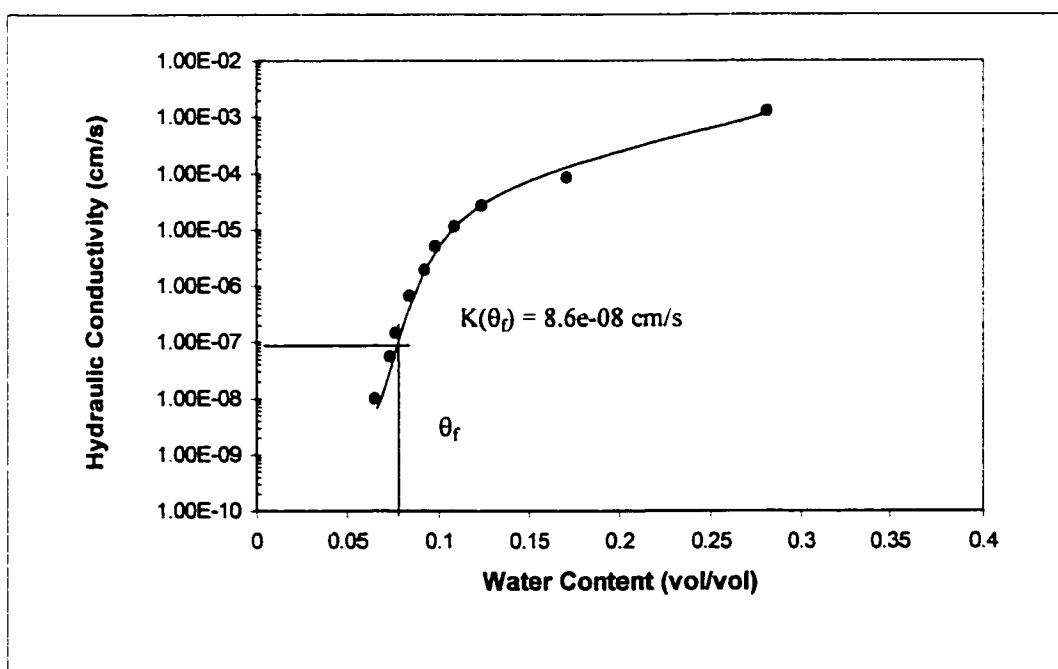


Figure 12f. $K(\theta)$ curve and $K(\theta_f)$ for sample C7.

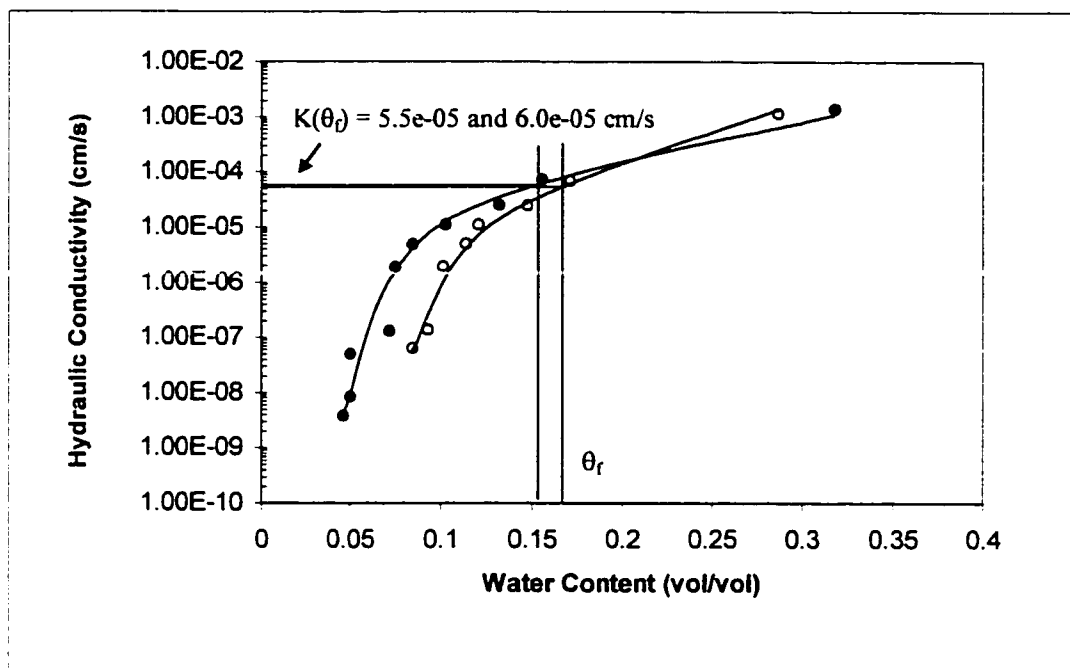


Figure 12g. $K(\theta)$ curve and $K(\theta_r)$ for sample C8-a (open circles) and C8-b (closed circles).

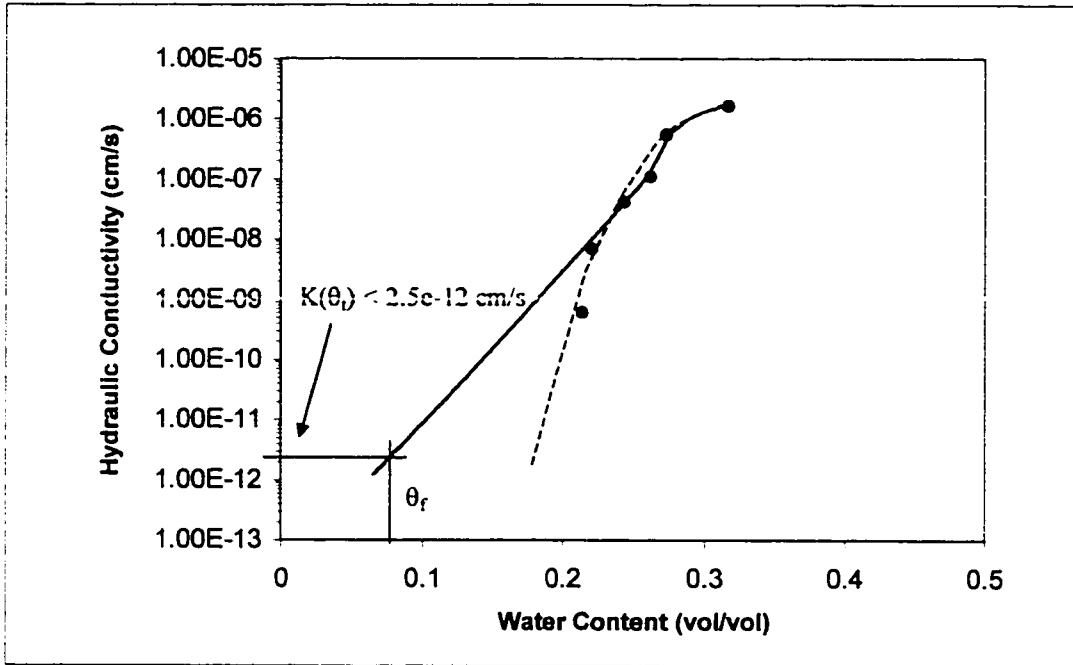


Figure 12h. $K(\theta)$ curve and extrapolation of estimated maximum $K(\theta_r)$ for sample T1 (dashed curve represents a trend that leads to a minimum $K(\theta)$ estimate and the solid curve represents a trend that leads to a maximum $K(\theta)$ estimate).

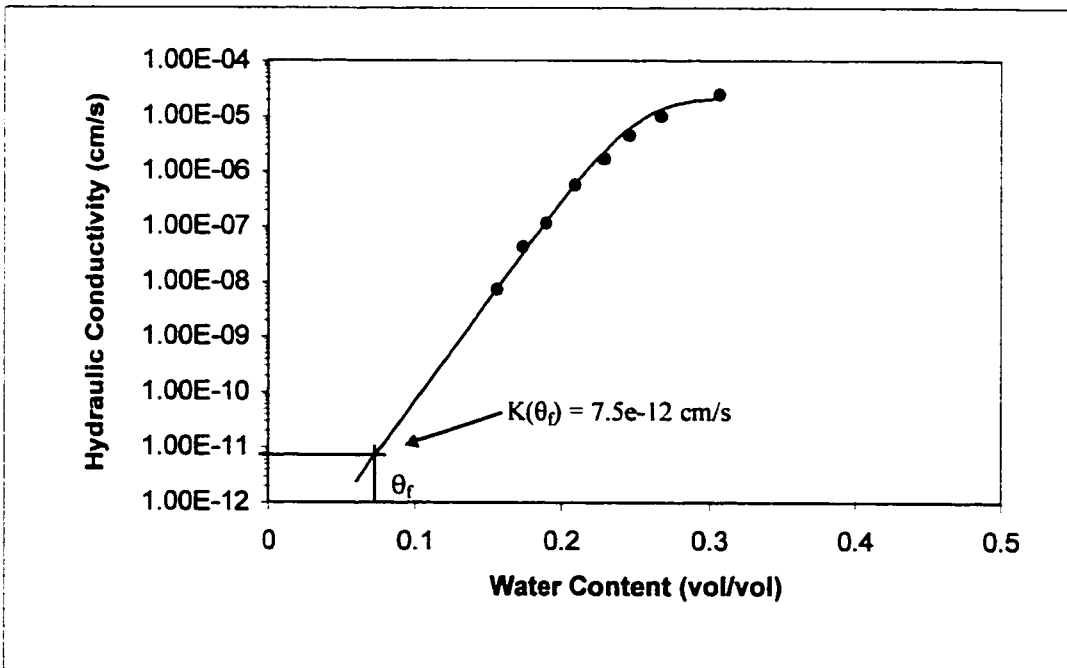


Figure 12i. $K(\theta)$ curve and extrapolation of estimated $K(\theta_r)$ for sample T2.

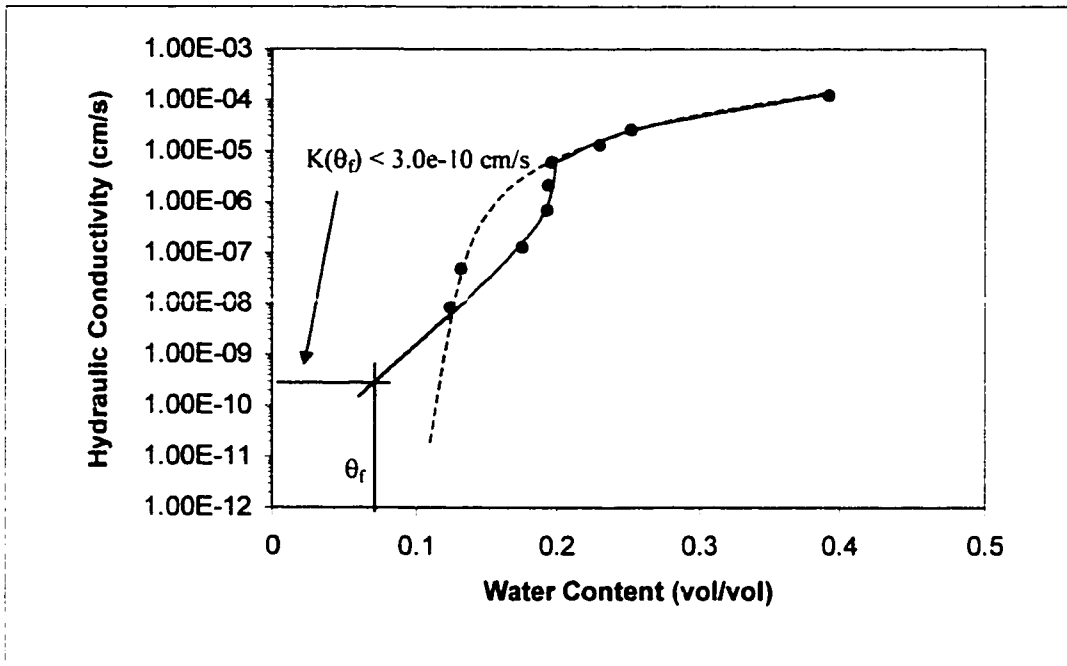


Figure 12j. $K(\theta)$ curve and extrapolation of estimated maximum $K(\theta)$ for sample T3 (dashed curve represents a trend that leads to a minimum $K(\theta)$ estimate and the solid curve represents a trend that leads to a maximum $K(\theta)$ estimate).

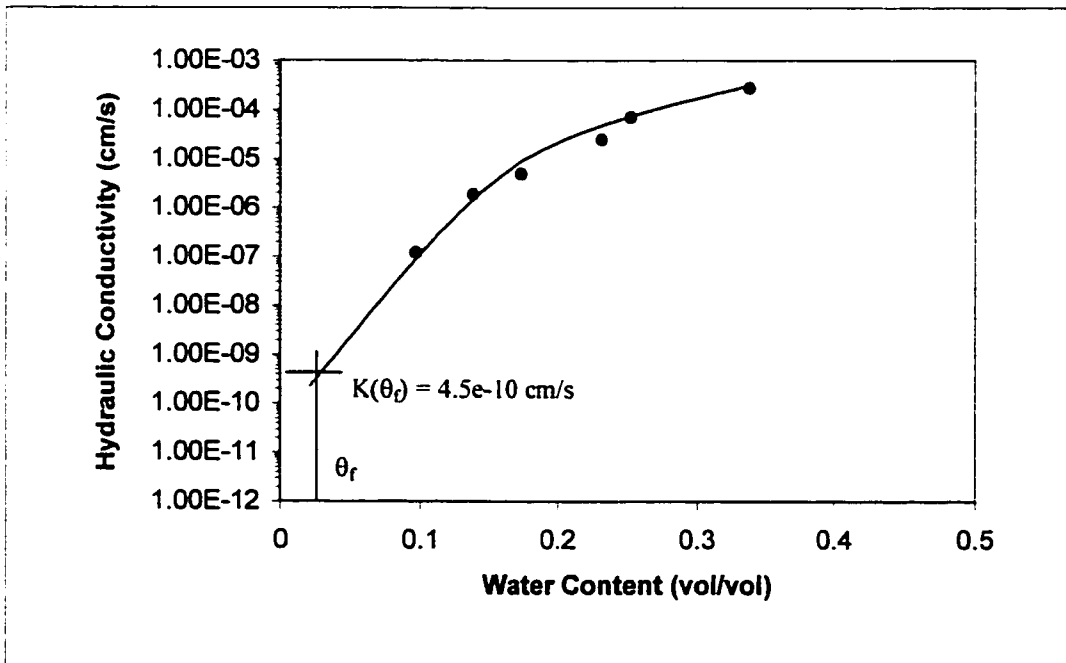


Figure 12k. $K(\theta)$ curve and extrapolation of estimated $K(\theta)$ for sample T4.

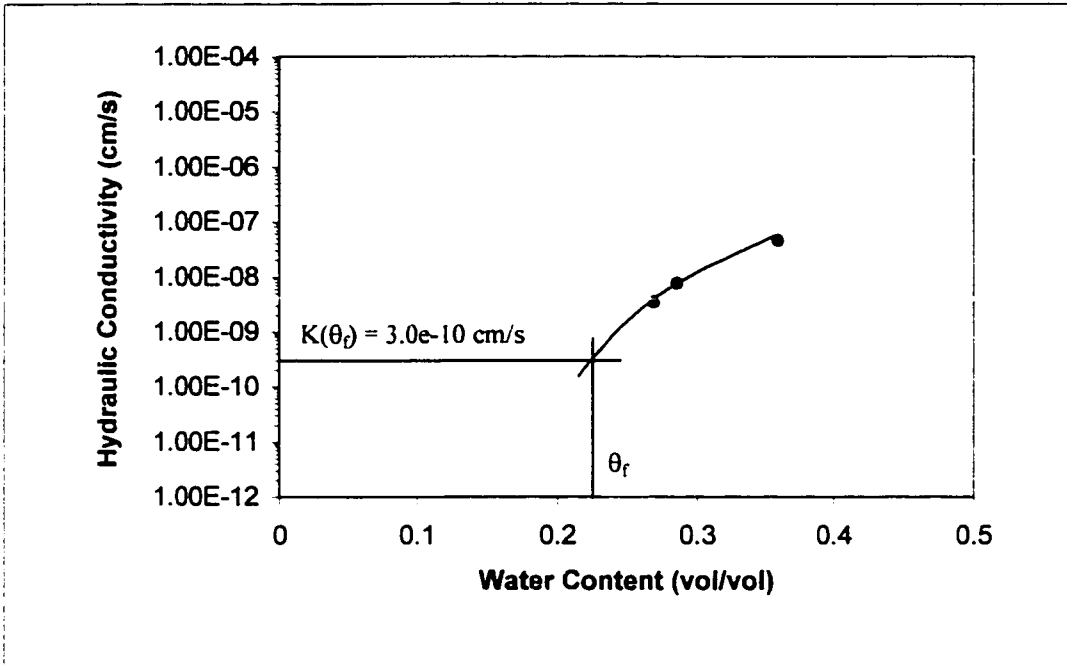


Figure 12l. $K(\theta)$ curve and extrapolation of estimated $K(\theta_r)$ for sample T5.

a trend that leads to a maximum extrapolated $K(\theta_f)$ estimate. The maximum extrapolated $K(\theta_f)$ estimates were used for this study.

Point Recharge Estimates

Provided core samples have been collected at depths sufficient to assume steady flow driven by gravity alone (Fig. 2), the $K(\theta_f)$ value determined for each sample directly indicates downward flux (q) at the location of the sample, which can be interpreted as a recharge rate. Table 4 shows a summary of core sample depths, $K(\theta_f)$ values (in cm/s) determined for each sample, and the associated inferred recharge rate (in cm/yr).

Table 4: Summary of sample depths, $K(\theta_f)$, and inferred recharge rate.

Borehole	Sample	Depth (m)	$K(\theta_f)$ (cm/s)	Recharge (cm/yr)
C1	a	0.4	1.5E-05	470
C1	b	0.5	1.9E-06	60
C1	c	1.9	7.3E-05	2300
C1	d	2.0	8.6E-05	2700
C2	-	2.6	6.1E-05	1900
C3	a	4.0	5.0E-09	0.16
C3	b	4.2	3.9E-09	0.12
C6	-	2.3	5.0E-06	160
C7	-	2.3	8.6E-08	2.7
C8	a	5.2	5.5E-05	1700
C8	b	5.4	6.0E-05	1900
T1	-	4.6	< 2.5E-12	< 0.000079
T2	-	5.4	7.5E-12	0.00024
T3	-	5.5	< 3.0E-10	< 0.0095
T4	-	5.4	4.5E-10	0.014
T5	-	5.1	3.0E-10	0.0095

- single sample collected from borehole

Comparison of $K(\theta_f)$ to C_u and D_{10}

Figures 13a, b, and c show graphical comparisons of C_u and $K(\theta_f)$ for channel cores, terrace cores and surface samples. Figures 14a, b, and c show graphical comparisons of effective particle size (D_{10}) and $K(\theta_f)$ for channel cores, terrace cores and surface samples. The scattered distribution of data points indicates that, as expected, neither the coefficient of uniformity nor effective particle size can be used as an indicator of $K(\theta_f)$ for this study.

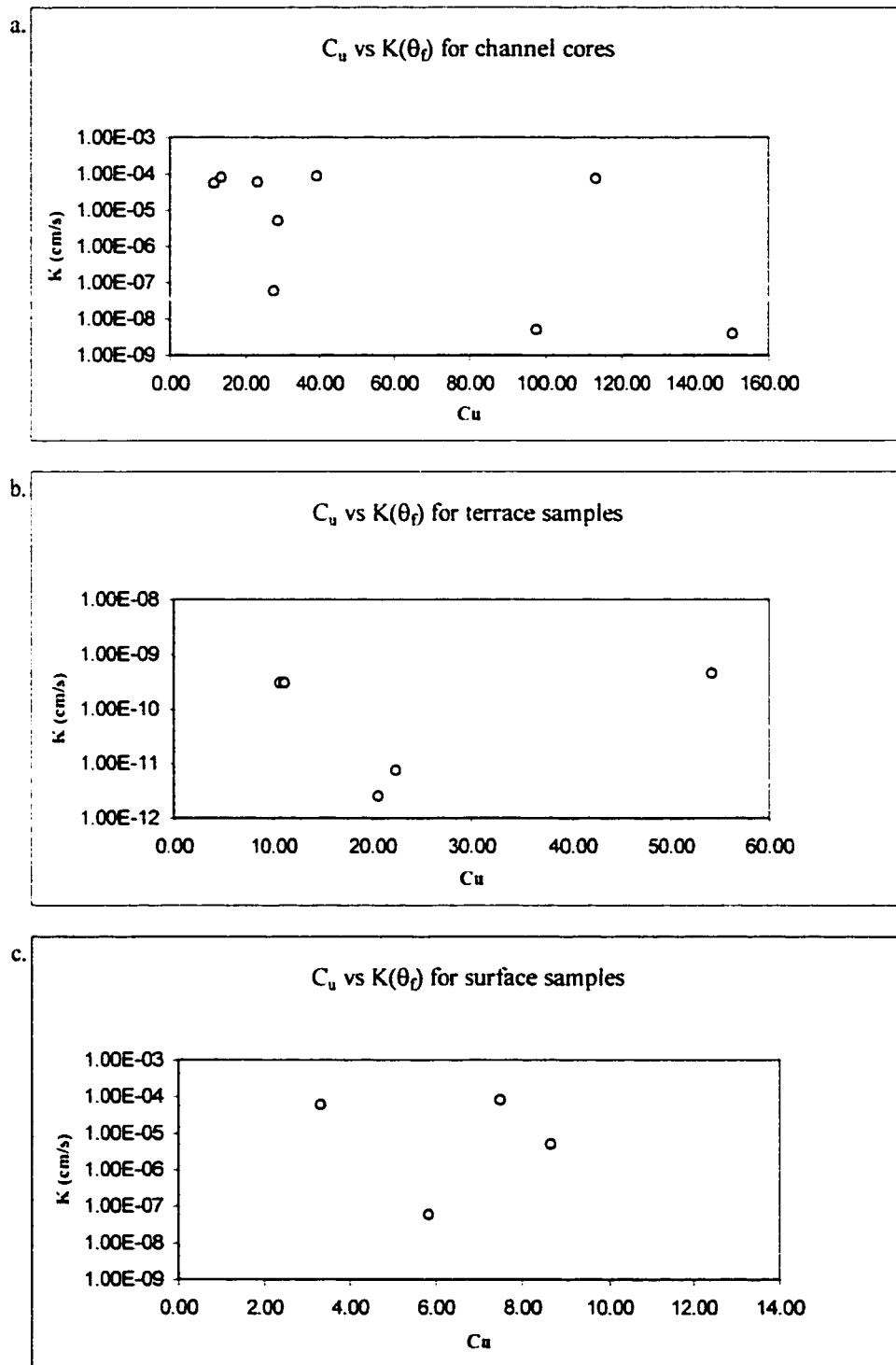


Figure 13. Comparison of C_u and $K(\theta_f)$ for a) channel cores, b) terrace cores, and c) surface samples.

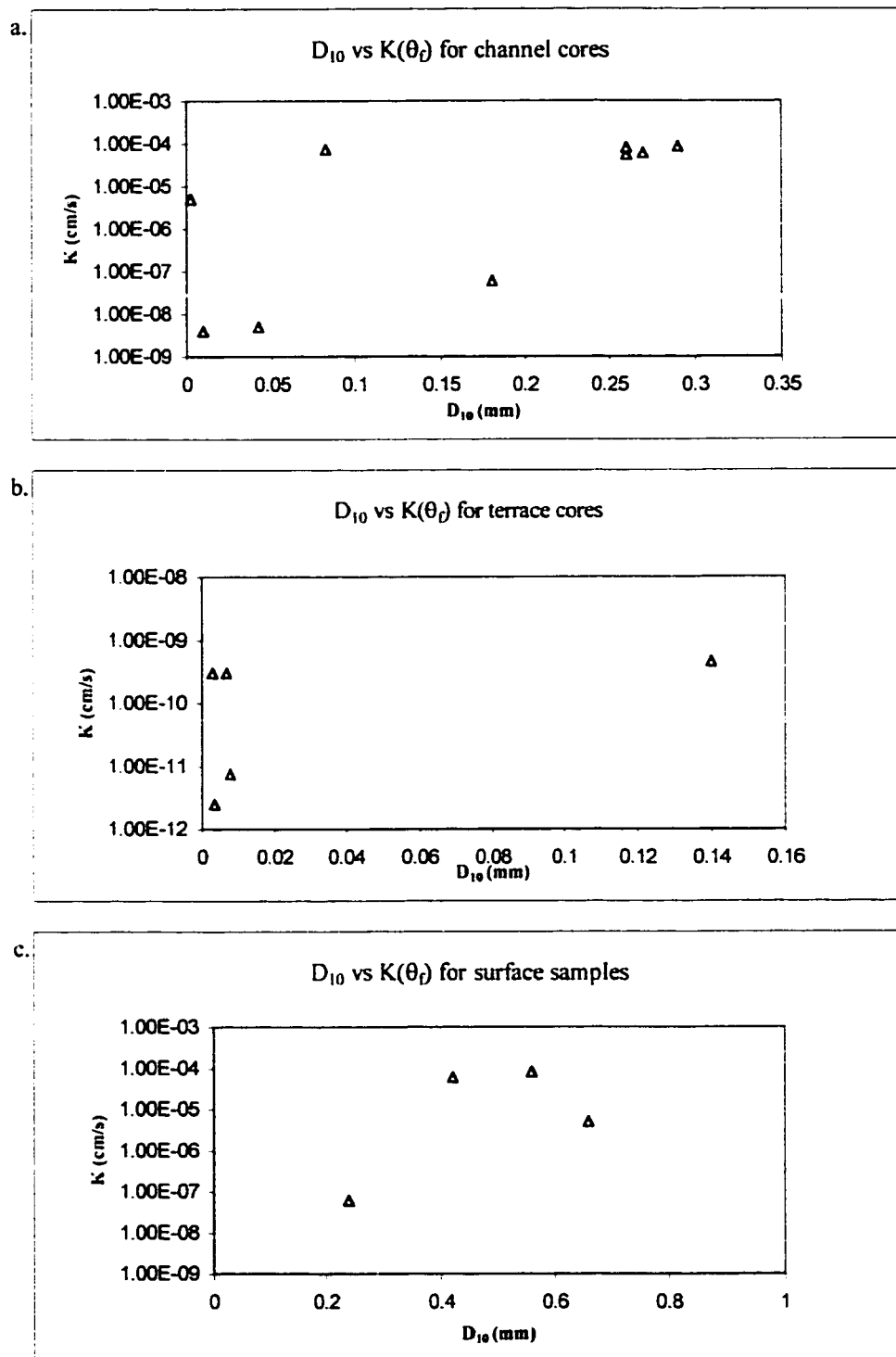


Figure 14. Comparison of D_{10} and $K(\theta_{\rho})$ for a) channel cores, b) terrace cores, and c) surface samples.

DISCUSSION

Depth to Steady Flow

Evidence for the depth that may be sufficient to infer steady flow driven by gravity alone is provided by four core samples taken from borehole C1, located at the upper reach of Abo Arroyo. Core samples C1-a and C1-b, taken at 0.4 and 0.5 m below the surface, show very different $K(\theta_f)$ values (1.5×10^{-5} and 1.9×10^{-6} cm/s). These values also differ significantly from $K(\theta_f)$ values for cores C1-c and C1-d taken at 1.9 and 2.0 m below the surface (7.3×10^{-5} and 8.6×10^{-5} cm/s). This variation with depth suggests that samples C1-a and C1-b are not deep enough to infer steady flow. However, the similarity of $K(\theta_f)$ values for samples C1-c and C1-d is consistent with a steady flow interpretation. Note that even though field water content differs for sample C1-c and C1-d, flux estimates are nearly equal, also consistent with the steady flow interpretation. Based on this evidence, the cores chosen for acceptable recharge rate estimates come from depths of at least 1.9 meters, i.e., core samples C1-a and C1-b are not deep enough to provide a long-term average recharge rate.

Although results of this study provide some evidence for the depth that may be sufficient to infer steady flow, no direct measurement of spatial and temporal variation in matric pressure could be obtained. It is possible that the downward flux estimates obtained in this study represent a transient downward flux rather than a long-term average recharge rate. Using data in this report, transient flow modeling could be used to

address this question. If modeling shows that these values represent transient downward fluxes rather than long term average recharge rates, further modeling could provide improved recharge estimates.

Channel Recharge

Figure 15 illustrates point recharge estimates at 6 locations within the channel of Abo Arroyo. Estimates for individual samples range from 0.12 to 2,700 cm/yr within the active channel. Samples taken from the upper reach, where streamflow is present much of the year, give q estimates of 1,900 to 2,700 cm/yr, with the exception of a 0.12 and a 0.16 cm/yr measurement obtained from a single borehole several meters farther down channel. Approximately 12 km down channel, q is estimated to be 160 cm/yr, and roughly 8 km farther down channel q is estimated to be 2.7 cm/yr, suggesting a marked decrease in recharge rate with distance down the arroyo. Recharge then appears to increase again to nearly 2,000 cm/yr, 28 km down-channel, near the confluence of Abo Arroyo and the Rio Grande.

The high recharge rates in the upper reach of Abo Arroyo probably result from frequent flows in combination with generally large sediment size. The low recharge rates of 0.12 and 0.16 cm/yr near the upper reach of Abo Arroyo may result from the lower permeability of sediment in this localized area. The core sample at C3 was taken at a location where fine sediment has accumulated and is not generally representative of this

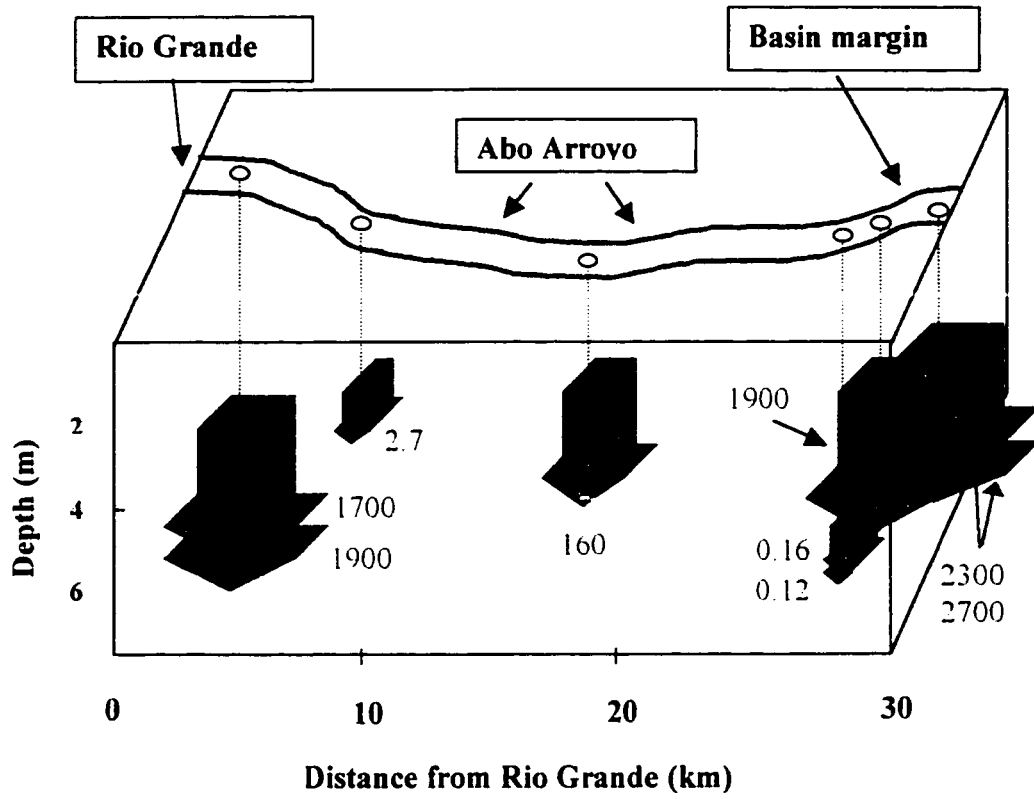


Figure 15. Variation in recharge rate (cm/yr) along the 30 km channel reach of Abo Arroyo.

portion of the arroyo with respect to bulk soil properties. As a result, this core sample can probably be considered anomalous with respect to its hydraulic properties as well. The middle portion of Abo Arroyo has lower recharge probably because of less frequent flows and smaller sediment size. Surface sediments through this area also display a hard crust that may inhibit infiltration and promote more surface flow down channel. The lower reach of Abo Arroyo has a high recharge rate similar to the upper reach. Factors that may contribute to increased recharge here include the high permeability of loose sandy sediment at this location and flow contributions from nearby tributaries, including possible inflow from nearby crop irrigation (see Fig. 7d).

A downward flux of up to 27 meters (2700 cm/yr at C1-d) of water per year through an arid-region arroyo may seem extremely high. However, the high flux density estimates come from core samples taken directly out of the active channel and come from the upper reach of Abo Arroyo where the greatest amount of infiltration likely occurs when water is present (i.e., during brief flow events that typically occur during summer months). Also, Abo Arroyo drains a relatively large watershed (~650 km²), consistent with significant infiltration through the arroyo. A rough quantitative analysis also suggests that the high estimates of point recharge are reasonable. Saturated conductivity values measured for channel samples where high point estimates have been obtained are as much as 1×10^{-3} cm/s, or equivalently, about 30,000 cm/yr. This is about the amount of recharge that would occur if water were present in the channel at this location for an entire year. A point recharge estimate of 2,700 cm/yr would require the presence of water 9% of the time, which seems reasonable.

Terrace Recharge

Figure 16 shows a comparison of inferred recharge rates in the channel of Abo Arroyo versus inferred recharge rates on the adjacent terraces. Recharge in the arroyo is significant, as described in the preceding section. In contrast, samples taken outside the arroyo, at distances of 3.5 to 465 m away, give q estimates of less than 0.015 cm/yr. Though the data set for terrace recharge estimates is somewhat limited, results show no consistent pattern of increasing or decreasing recharge rate with increasing distance from the channel. Recharge does appear to drop off abruptly outside the channel. The significantly lower recharge rate estimates outside the arroyo are consistent with the expectation of non-focused, areally-diffuse recharge typical of inter-arroyo regions. A recharge rate of 0.015 cm/yr applied over the entire MRGB (8000 km²) results in a total inter-arroyo recharge estimate of 970 acre-ft/yr.

Recharge rate estimates obtained at the same locations outside Abo Arroyo using a chloride mass balance (CMB) technique (Stonestrom and others, 1998) range from 0.004 to 0.19 cm/yr. Table 5 shows a comparison of terrace recharge rates obtained using the CMB technique and SSC method. Note that in both cases the recharge estimates are

Table 5: Comparison of terrace recharge rates obtained from CMB technique and SSC method.

Sample	Recharge (cm/yr)	
	CMB *	SSC
T1	0.19	<0.00008
T2	0.025	0.00024
T3	0.08	<0.0095
T4	0.065	0.014
T5	0.004	0.0095

* recharge values estimated from Figure 2 of Stonestrom and others, 1998

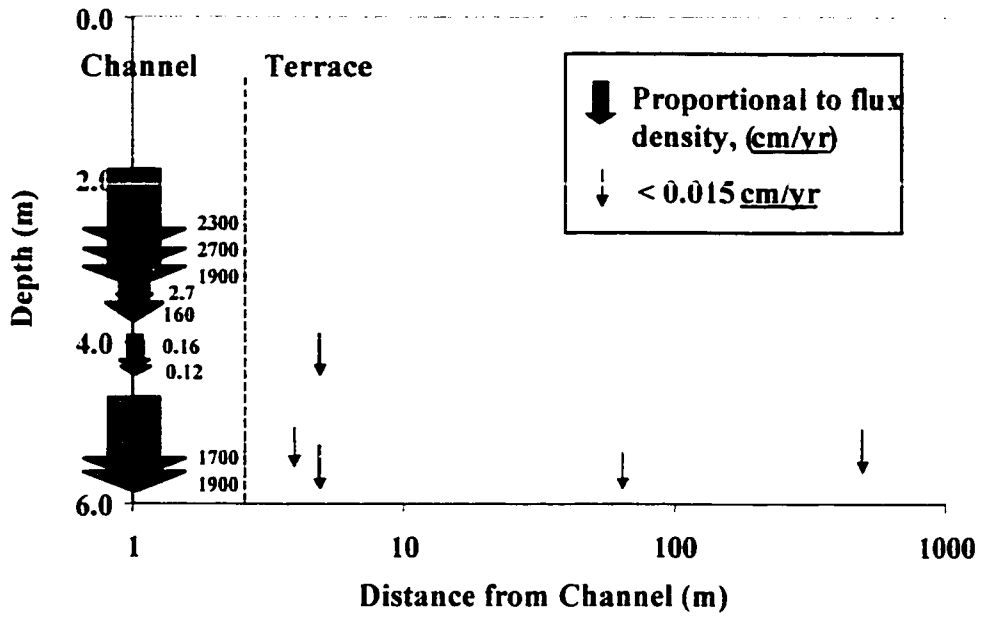


Figure 16. Comparison of terrace and channel recharge rates.

very low. However, if the largest recharge rate obtained using the CMB technique is applied to the entire MRGB, the resulting total recharge estimate for the entire MRGB is roughly 12,300 acre-ft/yr, slightly more than one order of magnitude greater than the 970 acre-ft/yr obtained using the largest SSC terrace recharge estimate.

Total Recharge Analysis

Using the point estimates of recharge rate at locations along the reach of Abo Arroyo, total recharge through the arroyo has been estimated by a combination of interpolation between measured point estimates and interpretation of geologic and hydrologic information. The amount of infiltration at a particular location within the arroyo is strongly influenced by two factors: 1) how readily water can infiltrate when it is present and 2) how frequently water is present at the particular location. Other factors, such as evapotranspiration, are believed to be minor. Note, however, that once water has infiltrated, factors such as evapotranspiration may be significant.

Results show reasonably good correlation between how readily water can infiltrate and effective particle size (Fig. 17, unpublished data from Amy Stewart). Based on this correlation, where possible, particle size and character of the sediment is used as an indicator of how readily water can infiltrate.

Effective particle size does not appear to be a good indicator of flow frequency. This may stem from the likelihood that sediment size in a given area is not only a result of flow frequency and volume, but also depends in part on reworking of previously

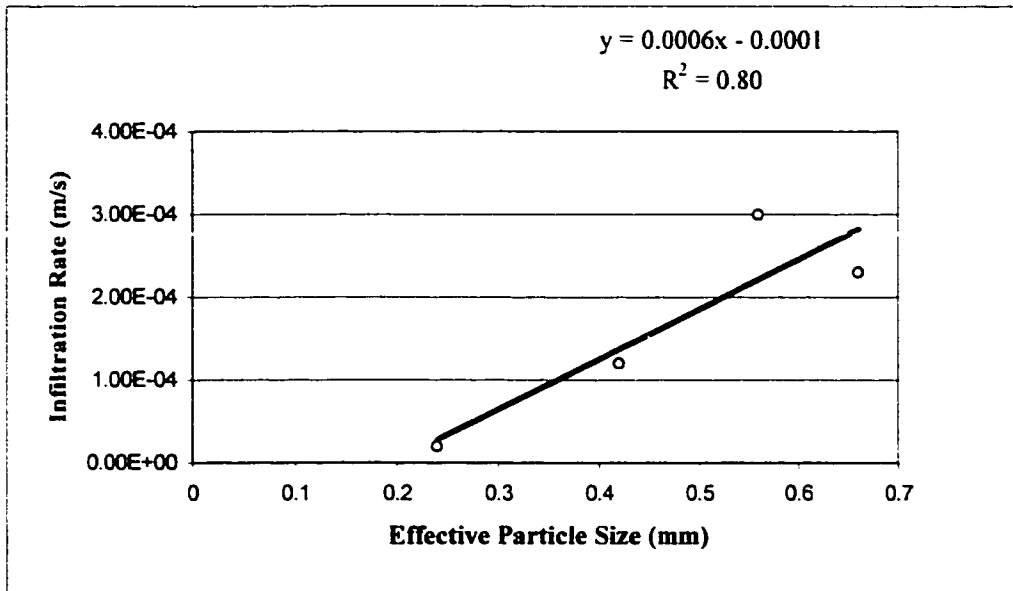


Figure 17. Infiltration rate as a function of effective particle diameter, D_{10} (unpublished data from Amy Stewart, 1998).

deposited sediment, possibly deposited under different geologic conditions. For this reason, larger scale geologic factors (e.g., the sedimentary environment through which Abo Arroyo passes) are used to interpret flow frequency. Interpretations are based on observations obtained from topographic maps, aerial photos, field notes, and previous studies of the site geology (Hawley and others, 1982; Spiegel, 1955; Titus, 1963; Machette, 1978).

Subregion Delineations

Abo Arroyo is inferred to flow through three geologic settings between the basin margin and the Rio Grande: the piedmont slope consisting of alluvial fan deposits sourced in the Manzano mountains, fluvial terraces of the ancestral Rio Grande, and the active floodplain of the Rio Grande. These differences in geologic environment delineate the primary subregions for the up-scaled point estimates based on the following analyses.

Subregion 1 – Rio Grande active floodplain. Based on aerial photos (Fig. 18), sample location C8 appears to be on the active floodplain of the Rio Grande. Aerial photos and topographic maps show a large erosional feature at the margin of the active floodplain, suggesting significant inflow from tributaries at this location, consistent with the high recharge estimates obtained. Nearby irrigation may contribute to or may be the primary source of flow into these tributaries. Also, loose, well-sorted sandy sediments predominate in this part of the arroyo, probably allowing for rapid infiltration when water

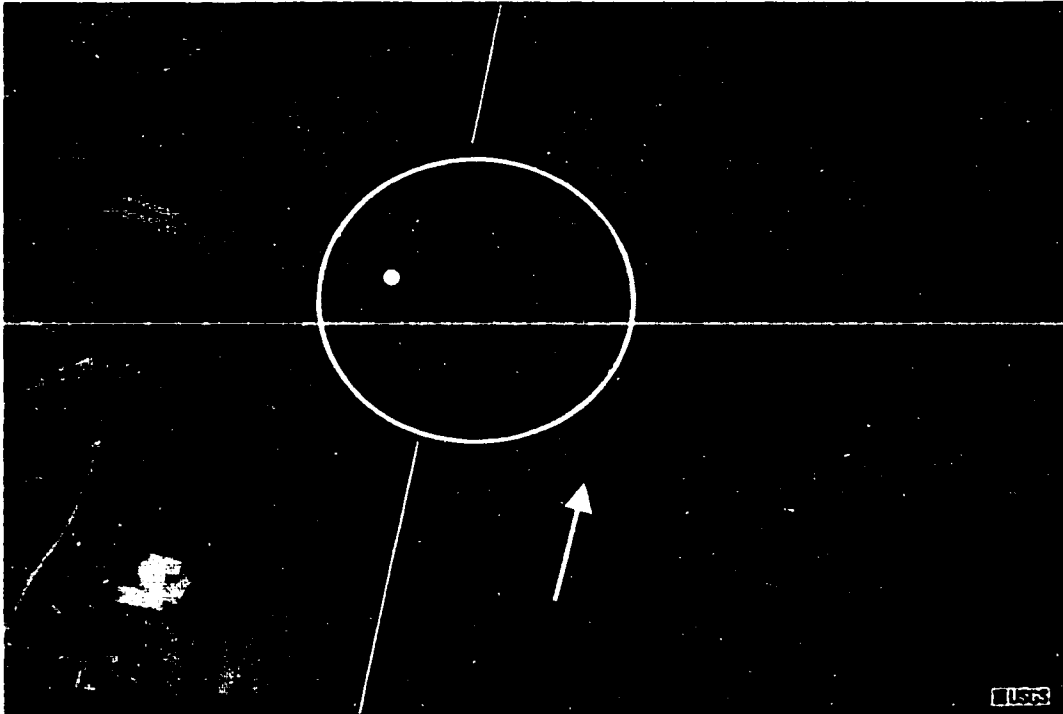


Figure 18. Aerial view of Abo Arroyo (arrow) showing transition from abandoned fluvial terraces to active floodplain of the Rio Grande (line), large erosional feature (oval), and location of borehole C8 (white dot).

is present. These observations suggest that the high recharge rate at this location is confined to a small area, 1 km in length, on the active Rio Grande floodplain. The average of two point estimates obtained from a single borehole (1700 and 1900 cm/yr) was assumed to apply throughout this subregion.

Subregion 2 - Fluvial terraces of the ancestral Rio Grande. Fluvial terraces of the ancestral Rio Grande extend for approximately 15 kilometers from the margin of the active Rio Grande floodplain to the west, to the distal portions of the Abo Canyon alluvial fan deposits to the east. Particle size analyses of surface samples (Abo 7) show well-sorted, sand-size sediment. However, in contrast to the loose sediment of the active floodplain subregion, a hard crust exists at this location that may reduce infiltration and promote more down-channel flow. It is plausible that the recharge rate obtained at borehole C7 (2.7 cm/yr) represents a typical recharge rate for the entire region of fluvial terraces of the ancestral Rio Grande. Given the limited data, the single point estimate of 2.7 cm/yr obtained in this subregion was applied to the entire subregion.

Subregion 3 – Piedmont slope. The third subregion is the piedmont slope, composed of alluvial fan deposits that extend 12 km westward from the basin margin (Hawley and others, 1982) to near the location of Abo 6. Particle size distributions of surface samples (Abo 3, 4, 6, 7, and 8) are consistent with a change in sedimentary environment near Abo 6. Surface samples Abo 7 and 8 are well sorted and fine grained when compared to surface samples Abo 3, 4, and 6, which display a bimodal distribution

and are coarser grained. It is plausible that a change from alluvial fan deposits to fluvial deposits of the ancestral Rio Grande 12 km down-channel from the basin margin coincides with a significant drop in flow frequency and volume through Abo Arroyo (i.e., alluvial fan deposits decrease and disappear where flow frequency and volume decrease significantly through Abo Arroyo), with relatively high recharge occurring through the piedmont slope subregion, and lower recharge occurring further down-channel.

On the upper portion of the fan, at the location of the basin margin, the recharge rate is estimated to be 2,000 cm/yr based on the following: Recharge estimates of 2,300 and 2,700 cm/yr were obtained from a single borehole (C1) located 1.4 km up-channel from the basin margin (see Table 4, Fig. 6). A recharge rate of 1,900 cm/yr was obtained from borehole C2 located approximately 0.3 km down-channel from the basin margin. Interpolation between an average recharge rate of 2,500 cm/yr 1.4 km up-channel from the basin margin and a recharge rate of 1,900 cm/yr 0.3 km down-channel from the basin margin yields an estimated recharge rate of 2,000 cm/yr at the basin margin itself.

Approximately 12 km down-channel from the basin margin, on the distal portion of the fan (location C6), the recharge rate is 160 cm/yr (Table 4). Because these estimates are from the proximal (basin margin) and distal portion of the fan, respectively, a reasonable total recharge estimate for the subregion could be obtained through interpolation. One might expect an exponential rather than linear decrease in flow frequency and volume with distance from the proximal part of the fan (Allen Gellis, 1998 pers. comm.). This is supported by the observation of a significant decline in largest sediment size with distance from the margin and a significant decline in slope of the

alluvial fan surface with distance from the margin. An exponential fit to the measured alluvial fan recharge estimates (Fig. 19a) produces the following equation:

$$R_1(x) = 20e^{-0.0002x} \text{ for } x = 0 \text{ to } 12,000 \text{ m}$$

where $R_1(x)$ represents recharge rate in cm/yr as a function of distance (x) from the proximal to the distal portion of fan. Integration of $R_1(x)$ multiplied by effective channel width provides an estimate of total recharge for this subregion and will be used for calculation of total recharge.

A second reasonable interpretation (though not used to calculate total recharge) regarding change in recharge rate along the reach of Abo Arroyo would be to assume that the change from piedmont facies to fluvial facies does not have a large effect on recharge, and it is distance from the basin margin that plays the primary role. An exponential fit to the alluvial fan and fluvial subregion recharge estimates (Fig. 19b) results in the equation:

$$R_2(x) = 28.241e^{-0.0003x} \text{ for } x = 0 \text{ to } 27,000 \text{ m.}$$

Integration of this equation over its respective interval results in essentially the same total recharge estimate.

Effective Channel Width

In addition to delineating subregions along the length of Abo Arroyo, the effective width of the subregions must also be estimated from available information. Measurements of active channel width, through use of aerial photos and field measurements at several locations along the reach of Abo Arroyo, show that the active

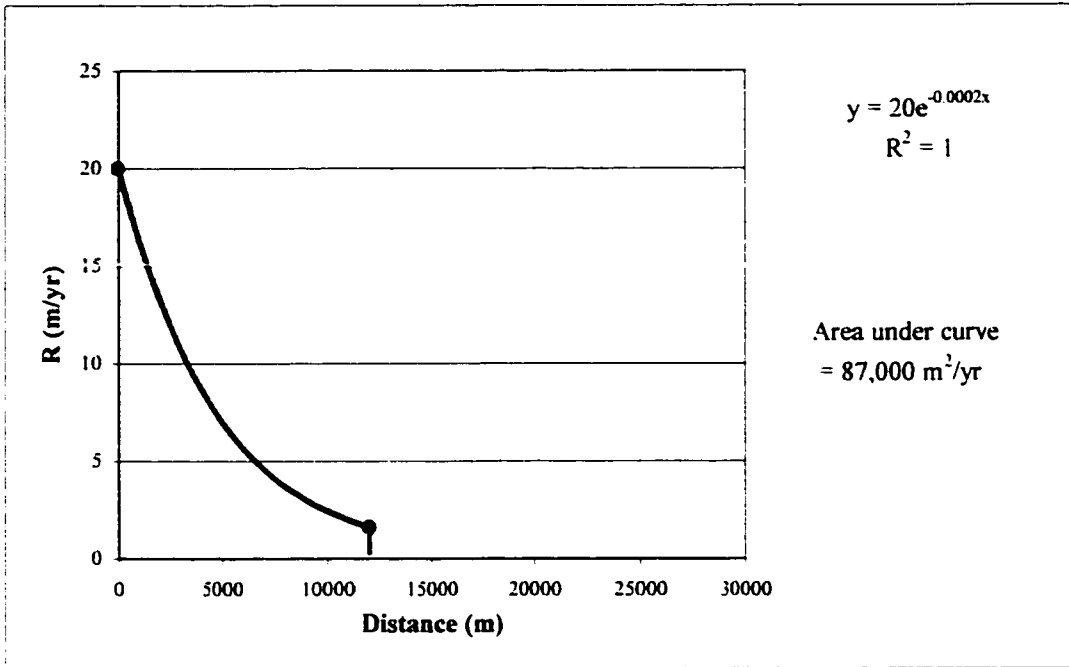


Figure 19a. Exponential fit to subregion 3 recharge estimates.

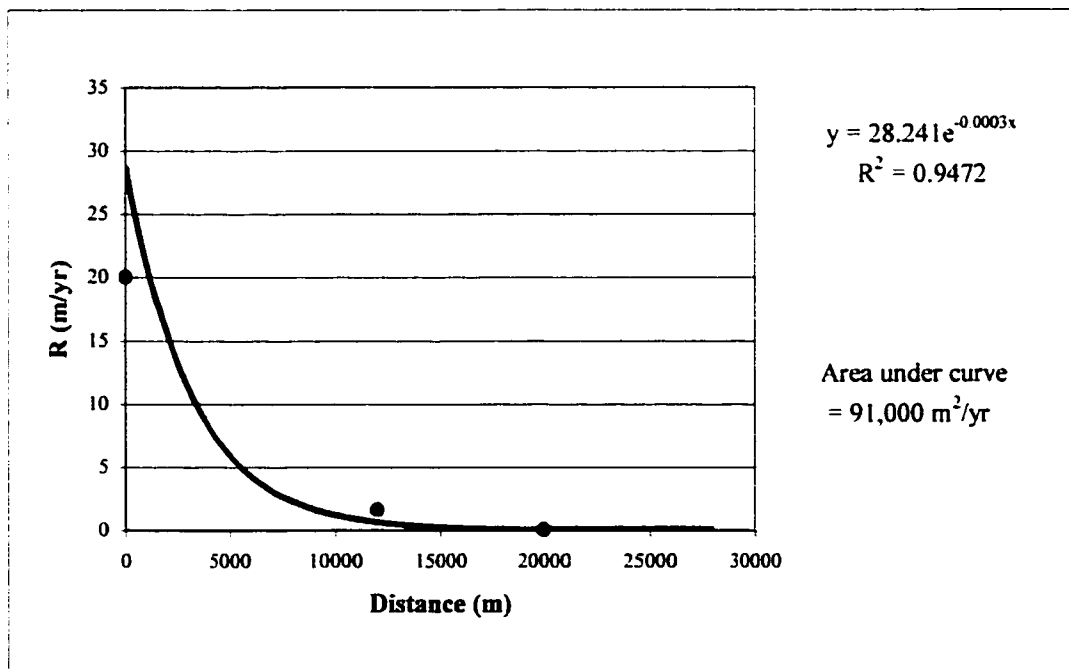


Figure 19b. Exponential fit to subregion 2 and subregion 3 recharge estimates.

channel is roughly 10 m wide along most of its length. However, as water percolates downward through the sediment during a flow event, lateral spreading will occur, increasing the effective channel width at the depth from which core samples were obtained (Fig. 20). Results of terrace recharge rate measurements (Fig. 16) suggest that recharge rate drops off abruptly outside the channel of Abo Arroyo, as noted above, and it is possible that the fine-textured sediments of the arroyo terrace deposits extend several meters below the surface of the arroyo channel. This would suggest that lateral flow is minimal below the channel surface. An analysis using the continuity equation also suggests that the effective channel width a few meters below the surface is on the order of five meters wider than the active channel, rather than tens of meters wider. The continuity equation states:

$$Q_{in} = Q_{out}$$

or

$$q_{in}A_{in} = q_{out}A_{out}$$

$$q_{in} \times \ell \times W_a = q_{out} \times \ell \times W_e$$

$$W_e = q_{in}/q_{out} \times W_a$$

with

Q_{in} : quantity of water per unit time moving into the system [L^3/T],

Q_{out} : quantity of water per unit time moving out of the system [L^3/T],

q_{in} : downward flux density into the system [L/T],

q_{out} : downward flux density out of the system [L/T],

A : cross sectional area [L^2],

ℓ : unit channel length [L],

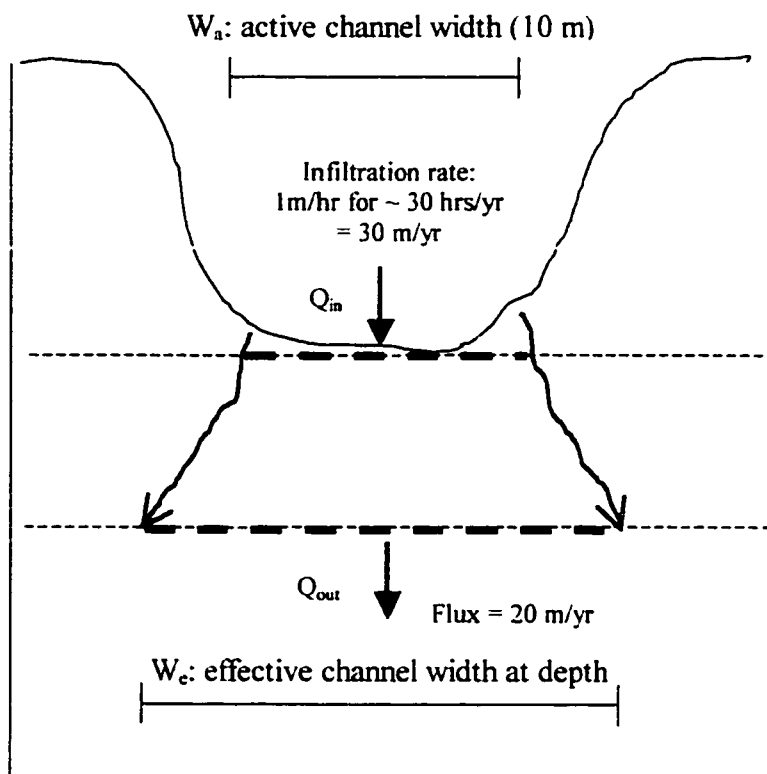


Figure 20. Diagram depicting lateral flow as water percolates downward and the resulting effective channel width at depth. See text for source of estimates of Q_{in} and Q_{out} .

W_a : active channel width [L],

W_e : effective channel width at the depth of the sample [L].

Effective channel width (W_e) can be computed given q_{in} , q_{out} , and W_a . In the upper reach of Abo Arroyo, the infiltration rate is roughly 1 m/hr when ponded (Amy Stewart, unpublished data). Assuming water is present in the channel for approximately 30 hours per year (6 significant flows per year lasting 4 to 6 hours each; Ortiz and others, 1997), the infiltration rate (q_{in}) is approximately 30 m/yr. With an active channel width of 10 meters, total annual downward flux at the channel surface (Q_{in}) is 300 m³/yr per meter of channel length. Given an annual flux density of about 20 m/yr (q_{out}) obtained from core samples collected 1.9 to 2.6 meters below the active channel surface in the upper reach of Abo Arroyo, effective channel width (W_e) must be 15 meters wide to maintain a 300 m³/yr downward flux at the depth of the core samples (Q_{out}):

$$W_e = (30 \text{ m/yr} / 20 \text{ m/yr}) \times 10\text{m} = 15\text{m}.$$

Note, however, that this analysis is highly speculative with regard to flow frequency and duration, and serves only to establish that the effective channel width a few meters below the surface is probably a few to several meters wider than the active channel width rather than tens of meters wider than the active channel width. This analysis also assumes no losses to evapotranspiration (which may be significant). This analysis cannot be readily applied down-channel without better knowledge of flow frequency and duration at those locations. Given the above analysis and limited data, an effective channel width of 15 m will be applied to all subregions.

Recharge Estimate

Table 6 summarizes the length, width, downward flux, and recharge estimate obtained for each subregion, and the sum total of recharge, approximately 1300 acre-ft/yr. These subregion delineations and recharge estimates are illustrated in Fig 21.

Table 6: Length, width, downward flux, and recharge estimate obtained for each subregion, and total recharge.

Sub-region	Length (km)	Width (m)	Recharge rate (m/yr)	Total recharge (acre-ft/yr)
1	1	15	18	220
2	15	15	0.03	5
3	12	15	$R_1(x)$	1070
Total	28	-	-	1295

Comparison to Other Studies

Figure 22 shows a comparison of total recharge estimates obtained by various methods. Estimates range from a high of 40,600 acre-ft/yr to a low of 900 acre-ft/yr. Whereas the 3 lowest estimates are plausible, the 2 highest recharge estimates are not. Stream gage data from 1997 show that total flow in Abo Arroyo at the mountain front is approximately 12,000 acre-ft/yr, far less than the 40,000 acre-ft/yr per year suggested by Waltemeyer (1994), and only slightly more than the 10,000 acre-ft/yr published by Kernodle and Scott (1986). Another type of rough estimate of total recharge through Abo Arroyo also suggests significantly less recharge. Assuming an average infiltration rate of 0.4 m/hr (Amy Stewart, unpublished data) over the length of the study reach (28 km), through a 10-meter-wide channel, the total infiltration for a six-hour event would be 550 acre-ft. Assuming 6 flow events per year gives a total recharge estimate of 3,300

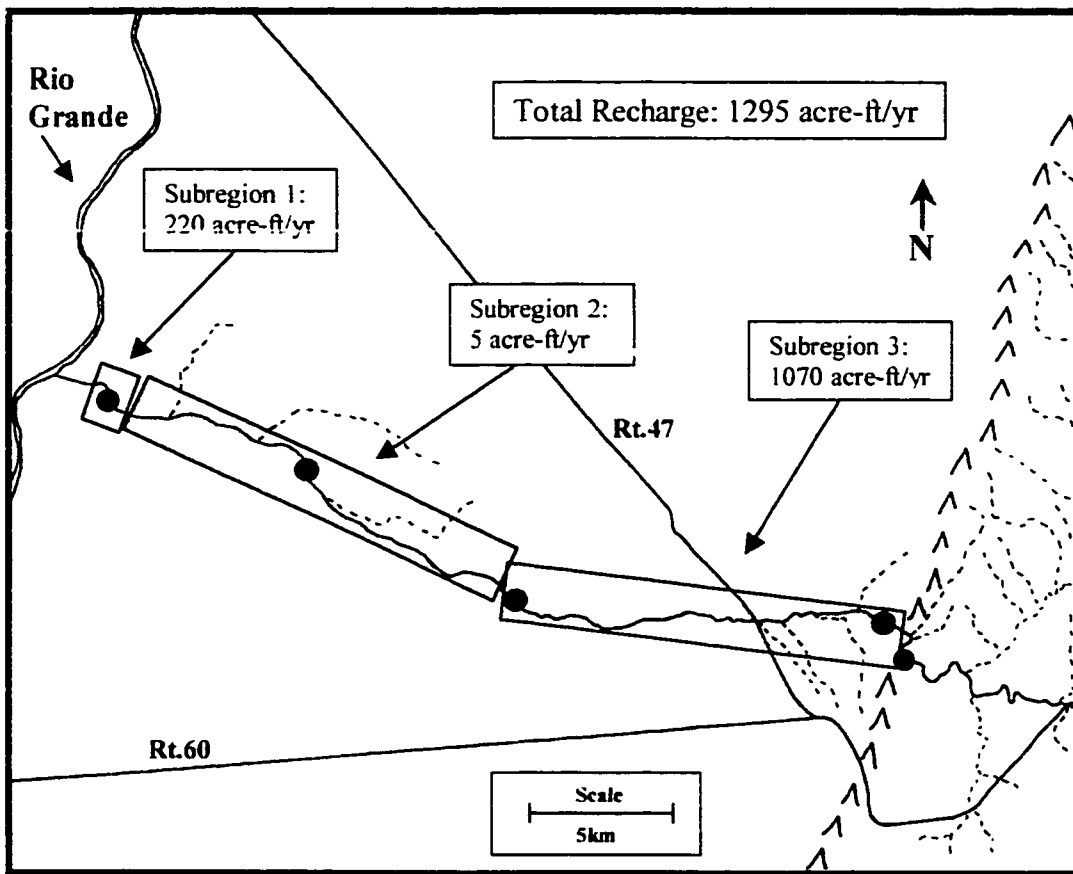


Figure 21. Subregion delineations and recharge estimates for each subregion.

Total Recharge

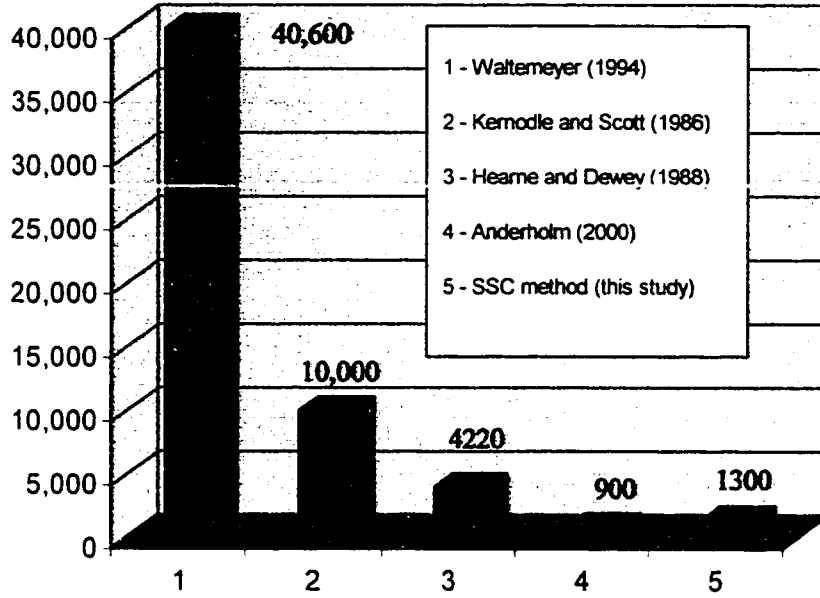


Figure 22. Comparison of total recharge estimates (acre-ft/yr) through Abo Arroyo.

acre-ft/yr, not including potential losses. Potential losses include evaporation, plant uptake of infiltrated water, and possible subsurface flow into the Rio Grande. The total recharge estimate for this study compares reasonably well with Anderholm's (2000) estimate of 900 acre-ft/yr for the channel of Abo Arroyo.

It is possible that the estimated recharge through the active floodplain subregion (subregion 1) results primarily from agricultural runoff, rather than runoff as a result of precipitation. If this subregion is discounted (as agricultural runoff is not accounted for in Anderholm's analysis), the total recharge estimate for this study is reduced to roughly 1100 acre-ft/yr.

Uncertainty in Upscaling

Upscaling of sparse point estimates to represent entire subregions of similar character is an ambiguous aspect of this study. Qualitatively, a comparison of particle size with measured hydraulic properties (unsaturated K and matric pressure) shows consistent patterns that would be expected, e.g., fine-textured samples consistently show relatively lower unsaturated hydraulic conductivity and more negative matric pressure for a given water content. However, results of this study show that no quantitative correlation can be readily made between easily measured or observed features of the site (such as effective particle size) and point recharge estimates. This stems from the fact that a measured recharge rate depends strongly on the field water content measured at the location of the sample. While field water content will vary as a function of particle size within the zone of steady flow, field water content also depends on the amount of water

available for infiltration into the unsaturated zone (i.e., flow frequency through the arroyo and the ability of water to infiltrate when present).

Uncertainty in Effective Channel Width

Because of uncertainty with regard to flow frequency and duration, and uncertainty with regard to sediment type more than 6 m below the terrace surface, there is uncertainty with regard to effective channel width at a depth several meters below the channel surface. The total recharge estimate would change by a percentage equivalent to the percent error in the effective channel width estimate. For example, if effective channel width at depth is in fact 20 m rather than 15m (an increase of 33%), then total recharge will be increased by 430 acre-ft/yr, resulting in an estimate for total channel recharge of roughly 1730 acre-ft/yr rather than 1300 acre-ft/yr.

CONCLUSIONS

Recharge rate measurements at several locations within and adjacent to Abo Arroyo have allowed for improved understanding of variation in recharge rate with location in the arroyo and improved understanding of the dependence of recharge rate on the local geologic environment. Results show that recharge in the upper reach of Abo Arroyo is significant (~2000 cm/yr). Several kilometers down-channel, recharge appears to be much less, ranging from 2.7 to 160 cm/yr. At the distal end of Abo Arroyo, near the confluence with the Rio Grande, recharge appears to increase again to nearly 2000 cm/yr. However, this high recharge rate is likely confined to a small area, and may be the result of runoff from crop irrigation. Whereas recharge is significant in Abo Arroyo itself, recharge appears to be negligible (<0.015 cm/yr) in the inter-arroyo regions adjacent to Abo Arroyo.

With the information obtained in this study, total recharge through Abo Arroyo has been estimated for comparison to other methods. The total recharge estimate obtained in this study (1300 acre-ft/yr) falls at the low end of the range of estimates found in previous studies. However, the total recharge estimate compares reasonably well with the study by Anderholm (2000), and an analysis using flow frequency, flow duration, and infiltration rates (Amy Stewart, unpublished data) suggests that recharge is likely a few thousand acre-ft/yr or less, rather than many thousand acre-ft/yr or more. Recharge through Abo Arroyo also appears to be significant when compared to total recharge within the inter-arroyo region of the MRGB. Inter-arroyo recharge is estimated to be 970

acre-ft/yr or less for the entire MRGB based on the results of this study. Abo Arroyo and its watershed cover 642 km² (roughly 1/12 the area of the MRGB), but recharge through this arroyo alone is estimated to be 1300 acre-ft/yr, representing a significant contribution to the MRGB

Results of this study also show that qualitative relationships between hydraulic properties and geologic information can be hypothesized, but quantifying these relationships with reasonable certainty requires more data.

REFERENCES CITED

- Anderholm, S. K., 2000, Mountain-front recharge along the eastern side of the middle Rio Grande Basin, Central New Mexico: U.S. Geological Survey Water Resources Investigation Report (in press).
- Blake, G.R., and Hartge, K.H., 1986, Particle Density, *in* Klute, A., ed., Methods of soil analysis, Part 1 – Physical and mineralogical methods, 2nd ed.: Madison, Wisconsin, Soil Science Society of America, Inc., Agronomy Series, n. 9, p. 377-381.
- Brooks, R.H., and Corey, A.T., 1964, Hydraulic properties of porous media: Hydrology Paper no. 3, Colorado State University, Fort Collins, Colorado, 27 p.
- Buckingham, E., 1907, Studies on the movement of soil moisture: United States Department of Agriculture Bureau of Soils, Bulletin 38, 61 p.
- Childs, E.C., 1969, An introduction to the physical basis of soil-water phenomena: John Wiley & Sons, London, England, 493 p.
- Gardner, W.R., 1964, Water movement below the root zone *in* Transactions of the 8th international congress of soil science, Bucharest, August 31 – September 9, 1964: Rompresfilatelia, Bucharest, p. 63-68.
- Hawley, J.W., Love, D.W., and Lambert, P.W., 1982, Road-log segment 1-C: Abo Canyon-Blue Springs area to Albuquerque via Belen and Los Lunas, *in* Grambling, J.A., and Wells, S.G., eds., Road-log from Albuquerque to Tijeras Canyon, Manzano, Abo Canyon, Rio Grande Estates, Canyon del Trigo, Belen, Los Lunas, and return to Albuquerque: New Mexico Geological Society Guidebook, 33rd Field Conference, Albuquerque Country II, p. 24-30.
- Hearne, G.A., and Dewey, J.D., 1988, Hydrologic analysis of the Rio Grande Basin north of Embudo. New Mexico, Colorado and New Mexico: U.S. Geological Survey Water Resources Investigation Report 86-4113, 244 p.
- Kernodle, J.M., McAda, D.P., and Thorn, C.R., 1995, Simulation of ground-water flow in the Albuquerque Basin, central New Mexico, 1901-1994, with projections to 2020: U.S. Geological Survey Water Resources Investigation Report 94-4251, 114 p., 1 pl.

- Kernodle, J.M., and Scott, W.B., 1986, Three-dimensional model simulation of steady-state ground water flow in the Albuquerque-Belen Basin, New Mexico: U.S. Geological Survey Water Resources Investigation Report 84-4353. 58 p.
- Klute, A., and Dirksen, C., 1986, Hydraulic conductivity and diffusivity: laboratory methods, *in* Klute, A., ed., *Methods of soil analysis, Part 1 – Physical and mineralogical methods*, 2nd ed.: Madison, Wisconsin, Soil Science Society of America, Inc., Agronomy Series, n. 9, p. 687-703.
- Machette, M.N., 1978, Preliminary geologic map of the Socorro 1 degree x 2 degree quadrangle, central New Mexico: U.S. Geological Survey Open-File Report 78-607, scale 1:250 000, 1 sheet.
- McAda, D.P., 1996, Plan of study to quantify the hydrologic relations between the Rio Grande and the Santa Fe Group aquifer system near Albuquerque, central New Mexico: U.S. Geological Survey Water Resources Investigation Report 96-4006. 58 p.
- Nimmo, J.R., Stonestrom, D.A., and Akstin, K.C., 1994, The feasibility of recharge rate determinations using the steady-state centrifuge method: *Soil Science Society of America Journal*, v. 58, p. 49-56.
- Ortiz, D., Lange, K., and Beal, L., 1997, Water resources data New Mexico water year 1997: U.S. Geological Survey Water-Data Report NM-97-1, p. 231.
- Spiegel, Z.E., 1955, Geology and ground-water resources of northeastern Socorro County, New Mexico: New Mexico Bureau of Mines and Mineral Resources Ground-Water Report 4, 99 p.
- Stonestrom, D.A., and Akstin, K.C., 1998, Environmental tracers of recharge at Abo Arroyo, Bear Canyon, and the Santa Fe River, middle Rio Grande Basin, New Mexico, *in* Slate, J.L., ed., *Middle Rio Grande Basin study- proceedings of the second annual workshop*, Albuquerque, New Mexico, February 10-11, 1998: U.S. Geological Survey Open-File Report 98-337, 91 p.
- Thorn, C.R., McAda, D.P., and Kernodle, J.M., 1993, Geohydrologic framework and hydrologic conditions in the Albuquerque Basin, central New Mexico: U.S. Geological Survey Water Resources Investigation Report 93-4149. 106 p.
- Titus, F.B., Jr., 1963, Geology and ground-water conditions in eastern Valencia County, New Mexico: New Mexico Bureau of Mines and Mineral Resources Ground-Water Report 7, 113p.

Waltermeyer, S.D., 1994, Methods for estimating streamflow at mountain fronts in southern New Mexico: U.S. Geological Survey Water Resources Investigation Report 93-4213, 17 p.